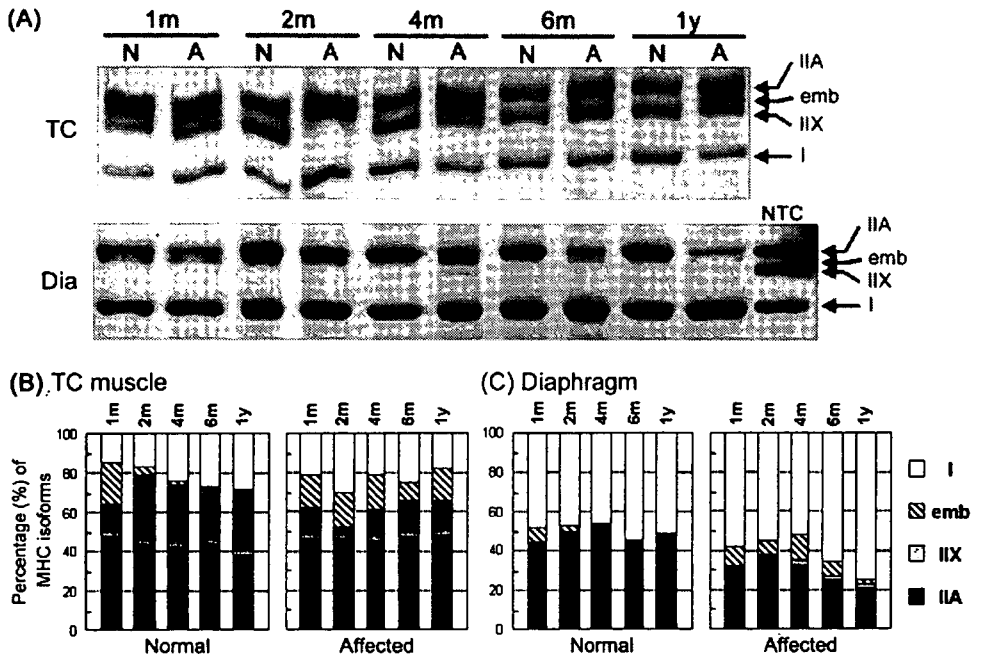


**Figure 7**

**MHC isoforms in skeletal muscles of normal and CXMD$_J$ dogs.** (A) Electrophoretic separation of MHC isoforms in TC muscle and diaphragm. Myosin was extracted from muscles at various ages (1, 2, 4, 6 months, and 1 year old), and aliquots of 0.4 μg of protein were separated on 8% SDS-polyacrylamide gels containing 30% glycerol. Four MHC isoforms (I, IIX, IIA, and embryonic) were detected. NTC: normal TC muscle at 1 year old. Note that MHC type I increased in the affected diaphragm after 6 months old. (B) Quantitative analysis of MHC isoforms. MHC expression between two groups (normal *vs* affected) or among ages (1, 2, 4, 6 months and 1 year) was analyzed by Yates's chi-square test. Significant differences ($p < 0.05$) were detected between normal and affected groups in TC muscles after 2 months old or in diaphragms after 4 months old, and between 1 and 2 months old in normal TC muscles.

regenerating fibers of the CXMD$_J$ diaphragm, the proportion of myofibers expressing slow type MHC increased markedly after 4 months old (Fig. 6C). These results suggested that MHC expression in TC muscle and the diaphragm of CXMD$_J$ would be influenced by different mechanisms after 4 months old. These age-dependent MHC expression might be related to body growth, particularly increasing of muscle mass. One possibility is participation of insulin-like growth factor (IGF)-1, which is important for postnatal growth of skeletal muscles [33] and can activate multiple $Ca^{2+}$-dependent signaling pathways, including the calcineurin/NFAT pathway [30]. When growth rate of body weight decreases after 4 months old [5], signaling activity of IGF-1 might reduce and MHC expression might be regulated predominantly by alternative signaling pathways.

***Comparison among mdx, CXMD$_J$, and DMD diaphragms***

MHC expression in normal skeletal muscle has been well studied in mice [15,34], dogs [11], and humans [35]. In normal dogs, the proportions of fiber types in TC muscle were relatively similar to those in the representative tibialis anterior muscles of mice and humans. In the diaphragm, however, the proportion of fiber types differed markedly among these species. The murine diaphragm is composed mainly of fast type IIA and IIX isoforms [15,34], but the canine diaphragm consists of equal populations of slow type MHC I and fast type MHC IIA [11], as also shown in our study. In normal human diaphragm, the distribution of myosin isoforms has been estimated that types I, IIA, and IIX account for approximately 45%, 40%, and 15%, respectively [35]. Thus, the proportions of MHC isoforms in the diaphragm of healthy dogs are much closer to those of humans than those of mice.

Some groups have studied expression profiles of MHC isoforms in the diaphragm of the *mdx* mouse. The *mdx* diaphragm shows increases in MHC type I fibers and elimination of type IIX population at 2 years old, but not at young ages (3 to 6 months old) [13,15,34]. In contrast to the *mdx* diaphragm, that in CXMD$_J$ exhibited drastic changes even in younger animals (6 months old). On the

other hand, there is no direct information available regarding the changes in fiber type composition in the diaphragm in human DMD. In addition, there is an important difference of MHC expression even in limb skeletal muscles between large mammals (including dogs and humans) and mammals with smaller body mass, especially rodents. The former do not express the fastest MHC IIB isoform in limb muscles [10,11,36], while it is abundantly expressed in the latter [34]. Therefore, changes/adaptations in skeletal muscles of dogs with muscular dystrophy are likely to be more relevant to human DMD, than that in the *mdx* mouse. As it is difficult to examine the diaphragms of DMD patients, it would be important to investigate the differences between murine and canine models for understanding the mechanisms of respiratory failure in human DMD.

## Conclusion

Based on fiber type classification using MHC expression, we demonstrated the predominant replacement with slow fibers and reduced muscle regeneration with progression of muscular dystrophy in the diaphragm of a canine DMD model, but these phenomena were much less strict in affected TC muscle. In addition, the expression profiles of MHC isoforms in the $CXMD_J$ diaphragm were evidently different from those of the *mdx* mouse. Our results indicated that dystrophic dog is a more appropriate model than a murine one for human DMD, and would be useful for investigation of the mechanisms of respiratory failure in DMD, as well as pathological and molecular biological backgrounds, and therapeutic effects in clinical trials.

## Competing interests

The author(s) declare that they have no competing interests.

## Authors' contributions

KY designed the study, carried out the pathological and immunohistological examinations, and drafted the manuscript. AN participated in interpretation of data, and helped to draft the manuscript. TH participated in coordination of the study. ST participated in the design, planning, and coordination of the study, and helped to draft the manuscript. All authors read and approved the final manuscript.

## Acknowledgements

We are grateful to Dr. Madoka Yoshimura, Dr. Nobuyuki Urasawa, Dr. Naoko Yugeta, Ms. Ryoko Nakagawa, and Dr. Masayuki Tomohiro for technical assistance. We also thank Mr. Hideki Kita and Mr. Shinichi Ichikawa for care and management of experimental animals. This work was supported by Grants-in-Aid for Center of Excellence (COE), Research on Nervous and Mental Disorders (13B-1, 16B-2, 17A-10, 19A-7), Health Science Research Grants for Research on Psychiatry and Neurological Disease and Mental Health (H12-kokoro-025, H15-kokoro-021, H18-kokoro-019), and the Human Genome and Gene Therapy (H13-genome-001, H16-genome-003) from the Ministry of Health, Labor, and Welfare of Japan, and Grants-in-Aid for Scientific Research to KY and High-Tech Research Center Project for Private Universities (matching fund subsidy, 2004-2008) from the Ministry of Education, Culture, Sports, Science, and Technology of Japan.

## References

1. Emery AEH: *Duchenne Muscular Dystrophy* 2nd edition. Oxford: Oxford University Press; 1993.
2. Nonaka I: **Animal models of muscular dystrophies.** *Lab Anim Sci* 1998, **48**:8-17.
3. Valentine BA, Cooper BJ, Cummings JF, De Lahunta A: **Canine X-linked muscular dystrophy: morphologic lesions.** *J Neurol Sci* 1990, **97**:1-23.
4. Howell JM, Fletcher S, Kakulas BA, O'Hara M, Lochmuller H, Karpati G: **Use of the dog model for Duchenne muscular dystrophy in gene therapy trials.** *Neuromuscul Disord* 1997, **7**:325-328.
5. Shimatsu Y, Yoshimura M, Yuasa K, Urasawa N, Tomohiro M, Nakura M, Tanigawa M, Nakamura A, Takeda S: **Major clinical and histopathological characteristics of canine X-linked muscular dystrophy in Japan, CXMDJ.** *Acta Myol* 2005, **24**:145-154.
6. Shimatsu Y, Katagiri K, Furuta T, Nakura M, Tanioka Y, Yuasa K, Tomohiro M, Kornegay JN, Nonaka I, Takeda S: **Canine X-linked muscular dystrophy in Japan (CXMDJ).** *Exp Anim* 2003, **52**:93-97.
7. Yugeta N, Urasawa N, Fujii Y, Yoshimura M, Yuasa K, Wada MR, Nakura M, Shimatsu Y, Tomohiro M, Takahashi A, Machida N, Wakao Y, Nakamura A, Takeda S: **Cardiac involvement in Beagle-based canine X-linked muscular dystrophy in Japan (CXMDJ): electrocardiographic, echocardiographic, and morphologic studies.** *BMC Cardiovasc Disord* 2006, **6**:47.
8. Fukushima K, Nakamura A, Ueda H, Yuasa K, Yoshida K, Takeda S, Ikeda S: **Activation and localization of matrix metalloproteinase-2 and -9 in the skeletal muscle of the muscular dystrophy dog (CXMDJ).** *BMC Musculoskelet Disord* 2007, **8**:54.
9. Yuasa K, Yoshimura M, Urasawa N, Ohshima S, Howell JM, Nakamura A, Hijikata T, Miyagoe-Suzuki Y, Takeda S: **Injection of a recombinant AAV serotype 2 into canine skeletal muscles evokes strong immune responses against transgene products.** *Gene Ther* 2007, **14**:1249-1260.
10. Scott W, Stevens J, Binder-Macleod SA: **Human skeletal muscle fiber type classifications.** *Phys Ther* 2001, **81**:1810-1816.
11. Toniolo L, Maccatrozzo L, Patruno M, Pavan E, Caliaro F, Rossi R, Rinaldi C, Canepari M, Reggiani C, Mascarello F: **Fiber types in canine muscles: myosin isoform expression and functional characterization.** *Am J Physiol Cell Physiol* 2007, **292**:C1915-1926.
12. Marini JF, Pons F, Leger J, Loffreda N, Anoal M, Chevallay M, Fardeau M, Leger JJ: **Expression of myosin heavy chain isoforms in Duchenne muscular dystrophy patients and carriers.** *Neuromuscul Disord* 1991, **1**:397-409.
13. Muller J, Vayssiere N, Royuela M, Leger ME, Muller A, Bacou F, Pons F, Hugon G, Mornet D: **Comparative evolution of muscular dystrophy in diaphragm, gastrocnemius and masseter muscles from old male *mdx* mice.** *J Muscle Res Cell Motil* 2001, **22**:133-139.
14. Lanfossi M, Cozzi F, Bugini D, Colombo S, Scarpa P, Morandi L, Galbiati S, Cornelio F, Pozza O, Mora M: **Development of muscle pathology in canine X-linked muscular dystrophy. I. Delayed postnatal maturation of affected and normal muscle as revealed by myosin isoform analysis and utrophin expression.** *Acta Neuropathol* 1999, **97**:127-138.
15. Petrof BJ, Stedman HH, Shrager JB, Eby J, Sweeney HL, Kelly AM: **Adaptations in myosin heavy chain expression and contractile function in dystrophic mouse diaphragm.** *Am J Physiol* 1993, **265**:C834-841.
16. Honeyman K, Carville KS, Howell JM, Fletcher S, Wilton SD: **Development of a snapback method of single-strand conformation polymorphism analysis for genotyping Golden Retrievers for the X-linked muscular dystrophy allele.** *Am J Vet Res* 1999, **60**:734-737.
17. Yuasa K, Sakamoto M, Miyagoe-Suzuki Y, Tanouchi A, Yamamoto H, Li J, Chamberlain JS, Xiao X, Takeda S: **Adeno-associated virus vector-mediated gene transfer into dystrophin-deficient skeletal muscles evokes enhanced immune response against the transgene product.** *Gene Ther* 2002, **9**:1576-1588.

18. Butler-Browne GS, Whalen RG: **Myosin isozyme transitions occurring during the postnatal development of the rat soleus muscle.** *Dev Biol* 1984, **102**:324-334.
19. Hosaka Y, Yokota T, Miyagoe-Suzuki Y, Yuasa K, Imamura M, Matsuda R, Ikemoto T, Kameya S, Takeda S: **Alpha1-syntrophin-deficient skeletal muscle exhibits hypertrophy and aberrant formation of neuromuscular junctions during regeneration.** *J Cell Biol* 2002, **158**:1097-1107.
20. Agbulut O, Li Z, Mouly V, Butler-Browne GS: **Analysis of skeletal and cardiac muscle from desmin knock-out and normal mice by high resolution separation of myosin heavy-chain isoforms.** *Biol Cell* 1996, **88**:131-135.
21. Webster C, Silberstein L, Hays AP, Blau HM: **Fast muscle fibers are preferentially affected in Duchenne muscular dystrophy.** *Cell* 1988, **52**:503-513.
22. Crow MT, Kushmerick MJ: **Chemical energetics of slow- and fast-twitch muscles of the mouse.** *J Gen Physiol* 1982, **79**:147-166.
23. Gramolini AO, Belanger G, Thompson JM, Chakkalakal JV, Jasmin BJ: **Increased expression of utrophin in a slow vs. a fast muscle involves posttranscriptional events.** *Am J Physiol Cell Physiol* 2001, **281**:C1300-1309.
24. Chakkalakal JV, Stocksley MA, Harrison MA, Angus LM, Deschenes-Furry J, St-Pierre S, Megeney LA, Chin ER, Michel RN, Jasmin BJ: **Expression of utrophin A mRNA correlates with the oxidative capacity of skeletal muscle fiber types and is regulated by calcineurin/NFAT signaling.** *Proc Natl Acad Sci USA* 2003, **100**:7791-7796.
25. Gregory P, Low RB, Stirewalt WS: **Changes in skeletal-muscle myosin isoenzymes with hypertrophy and exercise.** *Biochem J* 1986, **238**:55-63.
26. Dunn SE, Burns JL, Michel RN: **Calcineurin is required for skeletal muscle hypertrophy.** *J Biol Chem* 1999, **274**:21908-21912.
27. Allen DL, Sartorius CA, Sycuro LK, Leinwand LA: **Different pathways regulate expression of the skeletal myosin heavy chain genes.** *J Biol Chem* 2001, **276**:43524-43533.
28. Stupka N, Michell BJ, Kemp BE, Lynch GS: **Differential calcineurin signalling activity and regeneration efficacy in diaphragm and limb muscles of dystrophic *mdx* mice.** *Neuromuscul Disord* 2006, **16**:337-346.
29. Spangenburg EE, Booth FW: **Molecular regulation of individual skeletal muscle fiber types.** *Acta Physiol Scand* 2003, **178**:413-424.
30. Michel RN, Dunn SE, Chin ER: **Calcineurin and skeletal muscle growth.** *Proc Nutr Soc* 2004, **63**:341-349.
31. Valentine BA, Cooper BJ: **Canine X-linked muscular dystrophy: selective involvement of muscles in neonatal dogs.** *Neuromuscul Disord* 1991, **1**:31-38.
32. Chin ER, Olson EN, Richardson JA, Yang Q, Humphries C, Shelton JM, Wu H, Zhu W, Bassel-Duby R, Williams RS: **A calcineurin-dependent transcriptional pathway controls skeletal muscle fiber type.** *Genes Dev* 1998, **12**:2499-509.
33. Lupu F, Terwilliger JD, Lee K, Segre GV, Efstratiadis A: **Roles of growth hormone and insulin-like growth factor 1 in mouse postnatal growth.** *Dev Biol* 2001, **229**:141-162.
34. Coirault C, Lambert F, Marchand-Adam S, Attal P, Chemla D, Lecarpentier Y: **Myosin molecular motor dysfunction in dystrophic mouse diaphragm.** *Am J Physiol* 1999, **277**:C1170-1176.
35. Polla B, D'Antona G, Bottinelli R, Reggiani C: **Respiratory muscle fibres: specialisation and plasticity.** *Thorax* 2004, **59**:808-817.
36. Snow DH, Billeter R, Mascarello F, Carpene E, Rowlerson A, Jenny E: **No classical type IIB fibres in dog skeletal muscle.** *Histochemistry* 1982, **75**:53-65.


## Pre-publication history

The pre-publication history for this paper can be accessed here:

http://www.biomedcentral.com/1471-2474/9/1/prepub

STEM CELLS

TISSUE-SPECIFIC STEM CELLS

# Molecular Signature of Quiescent Satellite Cells in Adult Skeletal Muscle

SO-ICHIRO FUKADA,[a] AKIYOSHI UEZUMI,[a] MADOKA IKEMOTO,[a] SATORU MASUDA,[a] MASASHI SEGAWA,[b] NAOKI TANIMURA,[c] HIROSHI YAMAMOTO,[b] YUKO MIYAGOE-SUZUKI,[a] SHIN'ICHI TAKEDA[a]

[a]Department of Molecular Therapy, National Institute of Neuroscience, National Center of Neurology and Psychiatry, Tokyo, Japan; [b]Department of Immunology, Graduate School of Pharmaceutical Sciences, Osaka University, Osaka, Japan; [c]Bio and Nano Technologies, Science and Technology Division, Mizuho Information & Research Institute Inc., Tokyo, Japan

**Key Words.** Fluorescence-activated cell sorting • Microarray • Quiescence • Muscle satellite cells • Calcitonin receptor

ABSTRACT

**Skeletal muscle satellite cells play key roles in postnatal muscle growth and regeneration. To study molecular regulation of satellite cells, we directly prepared satellite cells from 8- to 12-week-old C57BL/6 mice and performed genome-wide gene expression analysis. Compared with activated/cycling satellite cells, 507 genes were highly upregulated in quiescent satellite cells. These included negative regulators of cell cycle and myogenic inhibitors. Gene set enrichment analysis revealed that quiescent satellite cells preferentially express the genes involved in cell-cell adhesion, regulation of cell growth, formation of extracellular matrix, copper and iron homeostasis, and lipid transportation. Furthermore, reverse transcription-polymerase chain reaction on differentially expressed genes confirmed that calcitonin receptor (CTR) was exclusively expressed in dormant satellite cells but not in activated satellite cells. In addition, CTR mRNA is hardly detected in nonmyogenic cells. Therefore, we next examined the expression of CTR in vivo. CTR was specifically expressed on quiescent satellite cells, but the expression was not found on activated/proliferating satellite cells during muscle regeneration. CTR-positive cells reappeared at the rim of regenerating myofibers in later stages of muscle regeneration. Calcitonin stimulation delayed the activation of quiescent satellite cells. Our data provide roles of CTR in quiescent satellite cells and a solid scaffold to further dissect molecular regulation of satellite cells.** STEM CELLS *2007;25:2448–2459*

Disclosure of potential conflicts of interest is found at the end of this article.

## INTRODUCTION

Muscle satellite cells, which account for 2%–5% of the total nuclei in adult skeletal muscle, play a major role in muscle regeneration [1, 2]. Under normal conditions, satellite cells are found external to the myofiber plasma membrane and beneath the muscle basal lamina [3] and are mitotically quiescent in the adult skeletal muscle [4, 5]. When activated by muscle damage, they proliferate, differentiate, fuse with each other or injured fibers, and eventually regenerate mature myofibers under the influence of innervation [6]. Recently, it was clearly demonstrated that the proliferation capacity of satellite cells in vivo is robust and that the contribution of interstitial cells or bone marrow-derived cells to muscle fiber regeneration is limited [7]. Importantly, a small fraction of activated satellite cells exit the cell cycle and return to the quiescent satellite state during muscle regeneration to maintain their numbers and the regenerative capacity of muscle.

Besides muscle fiber repair, satellite cells are also responsible for postnatal growth [8] and hypertrophy of skeletal muscle [9], and impairment of their functions is related to several pathological conditions, for example, muscular dystrophies and aging-related muscle atrophy [10]. Moreover, several studies showed that satellite cells differentiate into adipogenic cells or osteocytes in vitro [11–13], implying that they contribute to the fatty infiltration seen in Duchenne muscular dystrophy. Thus, normal functioning of satellite cells is indispensable for the integrity of skeletal muscle, and the cells themselves are an important source of cells for cell therapy of muscle diseases, making it valuable to clarify the molecular regulation of maintenance, activation/proliferation, and differentiation in satellite cells.

Like hematopoietic stem cells, most satellite cells are in a quiescent and undifferentiated state in the adult. Although quiescence is important to retain the proliferative and differentiative potential of satellite cells throughout the lifetime, the molecular regulation of quiescence remains poorly defined. Recent studies suggested that myostatin, a skeletal muscle-specific transforming growth factor-$\beta$ superfamily member, suppresses the activation of satellite cells [14]. Myostatin has been shown to induce a potent cyclin-dependent kinase inhibitor, p21(Cdkn1a), in vitro [15]. Other in vitro studies suggested that the decrease of MyoD protein and induction of another cyclin-dependent kinase inhibitor, p27(Cdkn1b) [16], and a Rb-related pocket protein, p130 [16, 17], are involved in the attainment of quiescence by proliferating myoblasts.

Correspondence: Yuko Miyagoe-Suzuki, M.D., Ph.D., Department of Molecular Therapy, National Institute of Neuroscience, National Center of Neurology and Psychiatry, 4-1-1 Ogawa-higashi, Kodaira, Tokyo 187-8502, Japan. Telephone: +81-42-346-1720; Fax: +81-42-346-1750; e-mail: miyagoe@ncnp.go.jp Received January 8, 2007; accepted for publication June 19, 2007; first published online in STEM CELLS *EXPRESS* June 28, 2007.  1066-5099/2007/$30.00/0 doi: 10.1634/stemcells.2007-0019

We previously reported a method to purify quiescent satellite cells from adult skeletal muscle using the fluorescence-activated cell sorting (FACS) technique and a novel antibody named SM/C-2.6 [18]. In this study, to clarify the molecular regulation of quiescent satellite cells, we performed genome-wide gene expression profiling of quiescent satellite cells isolated from C57BL/6 mice. Expression analysis of individual genes identified several candidate genes that regulate dormancy of satellite cells. Gene set enrichment analysis (GSEA) revealed that the gene sets involved in cell-cell adhesion, cell growth, copper and iron ion homeostasis, lipid transport, and formation of extracellular matrix were coordinately upregulated in quiescent satellite cells. Furthermore, we demonstrate that calcitonin receptor (CTR) is expressed specifically on quiescent satellite cells in vivo and that calcitonin significantly attenuates the activation of satellite cells. Our study is the first report of in-depth gene expression analysis of quiescent satellite cells and will greatly facilitate the investigation of molecular regulation of satellite cells in both physiological and pathological conditions.

## MATERIALS AND METHODS

### Animals

All procedures using experimental animals were approved by the Experimental Animal Care and Use Committee at the National Institute of Neuroscience. C57BL/6 mice were purchased from Nihon CLEA (Tokyo, http://www.clea-japan.com).

### Preparation of Satellite Cells and Nonmyogenic Cells from Mouse Limb Muscles

Mononuclear cells were prepared from fore- and hindlimb muscles of 8- to 12-week-old female C57BL/6 mice as described [19] and incubated on ice for 30 minutes in the presence of a 1:200 dilution of phycoerythrin-conjugated anti-CD45 (clone: 30-F11) and biotinylated SM/C-2.6 [18]. Cells were then incubated with streptavidin-labeled allophycocyanin on ice for 30 minutes and resuspended in phosphate-buffered saline (PBS) containing 2% fetal bovine serum (FBS) and 2 μg/ml propidium iodide (PI). Cell sorting was performed on a FACSVantage SE flow cytometer (BD Biosciences, San Diego, http://www.bdbiosciences.com). Dead cells were excluded by PI gating. All antibodies and reagents for FACS analysis were purchased from BD Pharmingen (San Diego, http://www.bdbiosciences.com/index_us.shtml).

### Cell Culture

Satellite cells were cultured in growth medium consisting of high-glucose Dulbecco's modified Eagle's medium (DMEM; Invitrogen, Carlsbad, CA, http://www.invitrogen.com) containing 20% fetal calf serum (FCS; Trace Biosciences, New South Wales, Australia), 2.5 ng/ml basic fibroblast growth factor (Invitrogen), and penicillin (100 U/ml)-streptomycin (100 μg/ml) (Gibco-BRL, Gaithersburg, MD, http://www.gibcobrl.com) on culture dishes coated with Matrigel (BD Biosciences). Single living myofibers were prepared as described [20] and transferred to Matrigel-coated 24-well culture dishes (one fiber per well). After a 2-day culture in growth medium with or without elcatonin, satellite cells that had detached from muscle fibers were counted.

### Immunocytochemical Analysis

FACS-sorted cells were collected on glass slides by Cytospin 3 (Thermo Shandon Inc., Pittsburgh, http://www.thermo.com) and immunostained as described [19]. Cultured cells were fixed on 8-well Lab-Tek Chamber Slides (Nunc, Rochester, NY, http://www.nuncbrand.com) and stained as described [19, 21] with mouse anti-Pax7 (1:100; clone: Pax7; Developmental Studies Hybridoma Bank, Iowa City, IA, http://www.uiowa.edu/~dshbwww), mouse anti-MyoD (1:200; clone: 5.8A; NeoMarkers; Lab Vision, Fremont, CA, http://www.labvision.com), mouse anti-myogenin (1:100; clone: F5D; Developmental Studies Hybridoma Bank), rabbit anti-Ki67 (1:2; Ylem, Rome), or rabbit anti-p57 antibodies (1:50; GeneTex, San Antonio, http://www.genetex.com) at 4°C overnight and then reacted with secondary antibodies conjugated with Alexa 488 or Alexa 568 (Molecular Probes, Eugene, OR, http://probes.invitrogen.com). Nuclei were stained with 4,6-diamidino-2-phenylindole (DAPI). Images were photographed using a phase-contrast and fluorescence microscope IX70 (Olympus, Tokyo, http://www.olympus-global.com) equipped with a Quantix air-cooled CCD camera (Photometrics, Kew, VIC, Australia, http://www.photometrix.com.au) and IP Lab software (Scanalytics, Rockville, MD, http://www.scanalytics.com).

### Immunohistochemistry

Immunostaining of muscle cryosections was performed as previously described [21] using rat anti-laminin α2 (1:200; clone 4H8-2; Alexis Biochemical, Lausen, Switzerland, http://www.axxora.com), rabbit anti-M-cadherin [21], rabbit anti-human CTR (1:200; Serotec Ltd., Oxford, U.K., http://www.serotec.com), goat anti-Notch 3 (1:100; R&D Systems Inc., Minneapolis, http://www.rndsystems.com), or mouse anti-Pax7. Rabbit anti-mouse HeyL polyclonal antibody was produced in our laboratory. In brief, the DNA fragment corresponding to amino acids 220-287 of mouse HeyL (GenBank: NM_013905) was fused to glutathione *S*-transferase in the pGEX-1 Lambda T vector (GE Healthcare, Uppsala, Sweden, http://www.gehealthcare.com). The purified fusion protein was used to immunize New Zealand White rabbits. The obtained serum was affinity-purified. For Pax7 staining, an M.O.M. kit (Vector Laboratories, Burlingame, CA, http://www.vectorlabs.com) was used to block endogenous mouse IgG. For CTR staining, horseradish peroxidase-conjugated anti-rabbit IgG donkey secondary antibody (1:100; GE Healthcare) and Alexa 568-conjugated Tyramid (Molecular Probes) were used to amplify the signal. Nuclei were counterstained with TOTO-3 (1:5,000; Molecular Probes) or DAPI. The images were recorded using a confocal laser scanning microscope system TCSSP (Leica, Heerbrugg, Switzerland, http://www.leica.com) or Axiophot microscope (Carl Zeiss, Jena, Germany, http://www.zeiss.com).

### Cell Cycle Analysis

Muscle-derived mononucleated cells or cultured SM/C-2.6 positive cells were suspended at $10^6$ cells per milliliter in DMEM (Invitrogen) containing 2% FBS (Trace Biosciences), 10 mM Hepes, and 10 μM Hoechst 33342 (Sigma-Aldrich, St. Louis, http://www.sigmaaldrich.com) and incubated for 45 minutes at 37°C. An additional incubation was performed in the presence of 10 μg/ml Pyronin Y (Sigma-Aldrich) for 45 minutes at 37°C. Cells were then washed with PBS containing 2% FCS. Muscle-derived mononucleated cells were stained with SM/C-2.6 antibody and analyzed by FACSVantage SE flow cytometer.

### Cell Proliferation Assay

After cell sorting, quiescent satellite cells were plated on 96-well culture plates at a density of 3,000-8,000 in the absence or presence of elcatonin (0.01-0.1 U/ml) (Asahi Kasei Pharma Corporation, Tokyo, http://www.asahi-kasei.co.jp/asahi/en) and cultured for 1-2 days. Then 5-bromo-2'-deoxyuridine (BrdU) (10 μM) was added to the culture. To examine the effects of elcatonin on activated satellite cells, satellite cells were cultured for 3 days and then elcatonin was added to the culture 24 hours before addition of BrdU. Twenty-four hours later, BrdU uptake was quantified by cell proliferation enzyme-linked immunosorbent assay, BrdU Kit (Roche Diagnostics, Basel, Switzerland, http://www.roche-applied-science.com), and lumi-Image F1 (Roche). In Figure 6B, cells were exposed to elcatonin for 30 minutes and washed twice with PBS and then plated on culture dishes.

### Detection of Apoptotic Cells

Cells were cultured on 8-well Lab-Tek chamber slides with or without elcatonin. Apoptotic cells were detected by rhodamine fluorescence using an ApopTag Red In Situ Apoptosis Detection Kit (Chemicon, Temecula, CA, http://www.chemicon.com).

### RNA Extraction and Reverse Transcription-Polymerase Chain Reaction

Total RNA was extracted from sorted or cultured cells with a Qiagen RNeasy Mini kit according to the manufacturer's instructions (Qiagen, Hilden, Germany, http://www1.qiagen.com) and then reverse-transcribed into cDNA by using TaqMan Reverse Transcription Reagents (Roche). The polymerase chain reaction (PCR) was performed with cDNA products under the following cycling conditions: 94°C for 3 minutes followed by 30–40 cycles of amplification, annealing, and extension (94°C for 15 seconds, 58°C for 30 seconds, and 72°C for 30 seconds) with a final incubation at 72°C for 5 minutes. Specific primer sequences used for PCR are described in supplemental online Materials and Methods.

### Target Synthesis, Gene Chip Hybridization, and Data Acquisition

To label antisense RNA (aRNA) with biotin for microarray hybridization, we followed the protocol supplied by the manufacturer (Affymetrix, Santa Clara, CA, http://www.affymetrix.com). Because the starting amount of total RNA was 100 ng for the sorted SM/C-2.6$^+$ cell fraction, we used a two-cycle biotin aRNA synthesis kit (Affymetrix). Labeled aRNA was fragmented according to Affymetrix GeneChip protocol and then hybridized to Affymetrix MOE430A GeneChip arrays for 16 hours. After washing, the gene chips were stained according to the instrument's standard Eukaryotic GE WS2v4 protocol using antibody-mediated signal amplification. The signal was determined, using the Microarray Suite (MAS) 5.0 absolute analysis algorithm, as the average fluorescence intensity among the intensities obtained from the probe set. The signal of a probe set was calculated as the one-step biweight estimate of combined differences of all the probe pairs (perfectly matched and mismatched) in the probe set. A one-sided Wilcoxon's signed rank test was used to calculate a $p$ value that reflects the significance of differences between perfectly matched and mismatched probe pairs. The $p$ value was used to make the absolute call for probe sets. A "Present" call was assigned to transcripts for $p$ values between 0 and .04, a "Marginal" call was assigned to transcripts for $p$ values between .04 and .06, and an "Absent" call was assigned to transcripts for $p$ values between .06 and 1.0.

### Microarray Data Analysis

Scanned output files were analyzed by the probe level analysis package MAS 5.0 (Affymetrix). The Present/Absent call provided by the Affymetrix programs was used for the first selection. The MAS 5.0-generated raw data were uploaded to GeneSpring software version 7.0 (Silicongenetics, Redwood, CA, http://www.chem.agilent.com/scripts/PHome.asp). Data normalization was achieved by one of two methods: (a) each signal was divided by the 50th percentile of all signals in a specific hybridization experiment or (b) each signal was divided by the median of its values in all samples. A more reliable list of "5-fold changing" genes was obtained by applying the filtering options of GeneSpring. Present calls in all (four) quiescent or activated satellite cell probes were selected and a restriction, which passed genes with raw data above 100, was applied. Then, using all the quiescent and activated satellite cells as data, we performed a one-way analysis of variance test between the quiescent satellite cell group and the activated satellite cell group. In particular, a parametric test, with variances assumed equal (Student's $t$ test, $p$ value cut-off .05; multiple testing correction: Benjamini and Hochberg false discovery rate), was applied. The genes passing all these filters and tests were selected as "5-fold changing genes." Nonmyogenic cells (SM/C-2.6$^-$/CD45$^-$ cells) were also prepared four times.

### Gene Set Enrichment Analysis

GSEA [22] is a statistical analysis of sets of gene expression profiles, separated by phenotypic labels. Using GSEA, we can test hypotheses concerned with predefined sets of genes; the rank orderings of the genes in the whole gene set calculated with a given ranking method are random with regard to a given classification of samples. As a result of the analysis, nominal $p$ values, family-wise error rate $p$ values, and false discovery rate (FDR) q values for test hypotheses (thus for gene sets) were obtained.

In our analysis, we used the GSEA-P software package [22], which is available from the Broad Institute (Cambridge, MA, http://www.broad.mit.edu). We prepared, as input to the GSEA-P, the MAS 5.0-generated raw signal data and gene sets derived independently. We chose genes on the chip that were detected (the Present call was assigned) in at least one sample (17,150 of 22,626). The raw signals of the chosen genes were normalized so that their total sum was 1. Because the total amount of mRNA in a quiescent satellite cell (QSC) is much less than that in an activated satellite cell (ASC), the normalized signal should be understood as a relative signal among the chosen genes. To compile the gene sets, we assigned each probe to a gene ontology (GO) category [23] using annotations of the MOE430A chip (September 22, 2005) provided by Affymetrix. Therefore, these gene sets reflect the structure of the GO categories and subcategories of molecular function (MF), biological process (BP), and cellular component (CC). The 17,150 genes chosen comprised 1,674, 1,698, and 412 gene sets in the MF, BP, and CC subcategories, respectively, and were reduced to 162, 218, and 85 after filtering out gene sets with sizes smaller than 20 or larger than 1,000. We ran the GSEA-P with the signal-to-noise option for its ranking metric, with permutation over phenotype labels of QSC and ASC samples, and repeated it 2,000 times with the "weighted" option for its scoring scheme.

## Results and Discussion

### Isolation of Quiescent Satellite Cells from Mouse Skeletal Muscle

First, to obtain RNA samples for microarray analysis, we prepared mononuclear cells from 8- to 12-week-old C57BL/6 mouse muscle, and the SM/C-2.6$^+$ fraction was collected as the satellite cell fraction by FACS [18] (Fig. 1A). Consistent with our previous report, more than 97% of fresh SM/C-2.6$^+$ cells expressed Pax7 (Fig. 1B) but were mostly negative for both MyoD (Fig. 1Ca, 1Cb) and Ki67 (Fig. 1Ce, 1Cf). After 4–5 days of culture, more than 98% of SM/C-2.6$^+$ cells expressed MyoD (Fig. 1Cg, 1Ch) and Ki67 (Fig. 1Ck, 1Cl). Both freshly isolated, uncultured SM/C-2.6$^+$ cells and SM/C-2.6$^+$ cells cultured in growth medium were negative for myogenin expression (Fig. 1Cc, 1Cd, 1Ci, 1Cj), but these cells started to express myogenin and differentiated well into multinucleated myotubes after mitogen withdrawal (data not shown). In contrast, more than 99% of freshly isolated SM/C-2.6$^-$/CD45$^-$ cells were negative for Pax7 expression (Fig. 1Bc, 1Bd), and cultured SM/C-2.6$^-$/CD45$^-$ cells did not express MyoD (data not shown), again indicating that myogenic cells are highly enriched in the SM/C-2.6$^+$ fraction.

The forward and side scatter profiles of freshly isolated SM/C-2.6$^+$ cells showed that they are small and uniform in granularity (data not shown). In fact, as shown in Figure 1D, the cell size of fresh SM/C-2.6$^+$ cells was estimated to be approximately one-half that of cultured SM/C-2.6$^+$ cells based on the forward scatter profile, indicating that the freshly isolated SM/C-2.6$^+$ cells were not activated yet. Pyronin Y staining showed the small amount of RNA content in freshly isolated SM/C-2.6$^+$ cells (Fig. 1D). In general, a Pyronin$^{low}$ and Hoechst 33342$^{low}$ fraction is considered

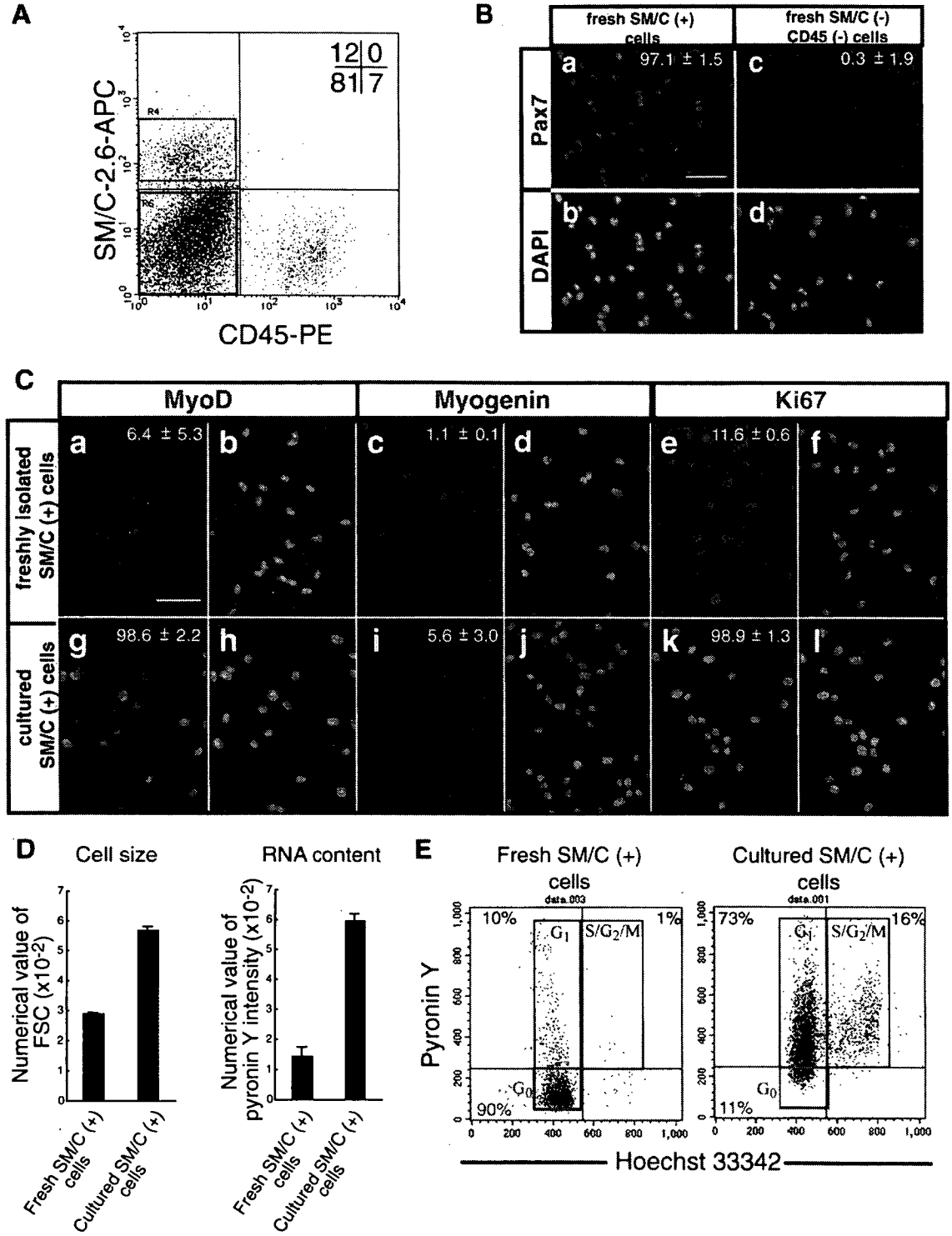


**Figure 1.** SM/C-2.6$^+$ cells isolated from skeletal muscle by fluorescence-activated cell sorting (FACS) are highly purified quiescent satellite cells and proliferate and express MyoD in culture. **(A):** Mononucleated cells prepared from uninjured limb muscles of adult mice were stained with anti-CD45 antibody and SM/C-2.6 monoclonal antibody. The SM/C-2.6$^+$ fraction (red square) and the SM/C-2.6$^-$/CD45$^-$ fraction (blue square) were collected for further analysis. **(B):** Freshly isolated SM/C-2.6$^+$ and SM/C-2.6$^-$/CD45$^-$ cells were stained with anti-Pax7 **(Ba, Bc)** antibody and DAPI **(Bb, Bd)**. The percentages of Pax7-positive cells in each cell fraction are shown. Cell fractionation was performed three times, and more than 300 cells from each fraction were counted. Scale bar: 50 μm. **(C):** Freshly isolated SM/C-2.6$^+$ cells and SM/C-2.6$^+$ cells cultured for 4 days in the presence of basic fibroblast growth factor were stained with antibodies to MyoD **(Ca, Cg)**, myogenin **(Cc, Ci)**, or Ki67 **(Ce, Ck)**. Percentages of MyoD-, myogenin-, or Ki67-positive cells are shown. Cell fractionation was performed three times, and more than 180 cells were counted each time. Nuclei were stained with DAPI **(Cb, Cd, Cf, Ch, Cj, Cl)**. Scale bar: 50 μm. **(D):** The mean value of FSC (cell size) and Pyronin Y intensity (RNA content) of freshly isolated SM/C-2.6$^+$ cells and satellite cells cultured in vitro. The value is an average of two independent experiments. **(E):** The percentages of cells in the G0 phase of the cell cycle were estimated by staining with Pyronin Y and Hoechst 33342. The number in the lower left of each FACS profile indicates the percentage of the G0 cells: 90% for fresh SM/C-2.6$^+$ cells and 11% for cultured SM/C-2.6$^+$ cells. Abbreviations: APC, allophycocyanin; DAPI, 4,6-diamidino-2-phenylindole; FSC, forward scatter; M, mitosis phase; PE, phycoerythrin; S, synthesis phase.

to be G0 cells [24]. Pyronin Y and Hoechst double staining shows that approximately 90% of fresh SM/C-2.6$^+$ cells were in the G0 phase of the cell cycle. In contrast, 90% of cultured SM/C-2.6$^+$ cells were cycling (Fig. 1E).

Thus, our procedure, which takes 5–6 hours in total to isolate 1–2 × $10^5$ SM/C-2.6$^+$ cells from one C57BL/6 mouse, enables us to isolate satellite cells still in a quiescent and undifferentiated state. The yield corresponds to 10%–15% of the total mononucleated cells obtained from mouse hind limb muscles by enzymatic digestion. Therefore, in this report, we call freshly isolated SM/C-2.6$^+$ cells "quiescent satellite cells" and cultured, proliferating SM/C-2.6$^+$ cells "activated satellite cells." Our procedure was also applicable to dystrophin-deficient *mdx* muscle with modifications, although 30%–40% of *mdx* satellite cells are Ki67-positive (M. Ikemoto et al., submitted manuscript). Unfortunately, SM/C-2.6 did not react with satellite cells from dystrophin-deficient dystrophic dogs (data not shown).

## Single Gene Analysis of Quiescent and Activated/Proliferating Satellite Cells

We prepared RNA samples from quiescent satellite cells and activated satellite cells and performed microarray analysis using Affymetrix GeneChips. Hybridization and data collection were performed four times using independent preparations of cells and RNA samples for each cell fraction. Raw data are available at http://www.ncbi.nlm.nih.gov/geo. The Gene Expression Omnibus accession number is GSE3483.

First, we compared the expression levels of individual genes in quiescent and activated states using GeneSpring software. We found that 507 genes (665 probes) were expressed in quiescent satellite cells at more than fivefold higher levels than in activated satellite cells (Fig. 2A). We roughly categorized these 507 genes into 11 gene groups: cell adhesion (15 genes), cell cycle regulation (26), proteolysis (21), cytoskeleton (13), cell surface (41), extracellular (61), immunoresponse (22), signal transduction (81), transcription (67), transport and metabolism (82), and unknown (78) based on Gene Ontology and listed all of them in supplemental online Table 1. On the other hand, 659 genes (814 probes) were upregulated (>fivefold) in the activated state (supplemental online Table 2). We also examined the gene expression of proliferating satellite cells/myoblasts in vivo that were directly isolated from regenerating muscle 2 days after cardiotoxin injection. The activated and proliferating satellite cells in vivo showed an expression profile quite similar to satellite cells cultured in vitro (data not shown).

## Upregulation of Cell Cycle Regulators in Quiescent Satellite Cells

Under normal conditions, most satellite cells are in the G0 phase of the cell cycle, possibly preventing their premature exhaustion. It is of note that nine genes encoding negative regulators of the cell cycle were highly upregulated in the quiescent stage: *Rgs2* (*regulator of G-protein signaling 2*) (×69, ×23), *Rgs5* (×37, ×21), *Pmp22* (*peripheral myelin protein 22*)/*Gas3* (growth arrest specific 3) (×25), *Cdkn1c* (cyclin-dependent kinase inhibitor 1C)/*p57* (×14), *Spry1* (sprouty homolog 1) (×11), *Gas1* (×7, ×6), *Reck* (reversion-inducing-cysteine-rich protein with kazal motifs) (×6), *Ddit3* (DNA-damage inducible transcript 3) (×6), and *Trp63* (transformation-related protein 63) (×5) (supplemental online Table 1). Reverse transcription (RT)-PCR confirmed that *Rgs2*, *Pmp22*, *p57*, and *Spry1* are highly expressed in quiescent satellite cells and downregulated in activated satellite cells (Fig. 2Ba).

Cyclin-dependent kinase inhibitors (CKIs) play a key role in controlling the cell cycle in many cell types. p21 (CIP1) triggers the cell cycle exit of proliferating myoblasts to initiate myoblast terminal differentiation in response to differentiation signals [25]. p57 (KIP2) is induced in myoblasts upon differentiation. Gene targeting experiments showed that these two CKIs redundantly control cell cycle exit during myogenesis [26]. Compared with irreversible cell cycle arrest upon differentiation, however, attainment of a reversible G0 state by satellite cells is poorly understood. In vitro studies suggested that Rb family members p130 and p27 are involved in the reversible cell cycle exit of proliferating myoblasts to return satellite cells to quiescence [16]. In our experiments, p21 (×0.5), p27 (×1.5), and p130 (×2–3) were not significantly upregulated in quiescent satellite cells. Reflecting the levels of p57 mRNA, p57 protein was found in more than 90% of freshly isolated SM/C-2.6$^+$ cells (Fig. 2Ca). Whether p57 is required for acquisition and maintenance of quiescence of satellite cells remains to be determined in a future study.

## Upregulation of Myogenic Inhibitors in Quiescent Satellite Cells

Quiescent satellite cells barely express myogenic basic helix-loop-helix (bHLH) factors. Activity of the *Myf-5* locus was revealed through a reporter gene, but Myf-5 protein is hardly detected in dormant satellite cells. On activation, satellite cells upregulate Myf5 and start to express MyoD [27] (Fig. 1). Our microarray analyses revealed that several myogenic inhibitory molecules were upregulated in quiescent satellite cells: *Bmp6* (*bone morphogenetic protein 6*) (×214), *Bmp4* (×66), *Bmp2* (×82), *Heyl* (*hairy/enhancer-of-split related with YRPW motif-like*)/*Herp3*/*Hrt3*/*hesr3* (×101, ×33, ×32), *Musculin*/*MyoR* (×83), *Notch3* (×9). Upregulation of *Bmp4*, *Bmp6*, *Msc*/*MyoR*, and *Heyl* in quiescent satellite cells was confirmed by RT-PCR (Fig. 2Bb). BMP4 is reported to negatively regulate MyoD expression in somite myogenesis [28] and differentiation of satellite cells, where BMP4-induced inhibition of myogenic differentiation requires Notch signaling [29]. Notch signaling is reported to inhibit the differentiation of myoblasts by repression of MyoD expression [30]. In postnatal muscle, Notch signaling controls satellite cell activation and their cell fate [31], and insufficient upregulation of the Notch ligand Delta is casually related to impaired regeneration of aged muscle [32]. Among several molecules in the Notch signaling pathway, our microarray analysis showed that *Notch3* and one of the Notch-effector genes, *Heyl*, are highly expressed in quiescent satellite cells. When cross-sections of normal mouse tibialis anterior (TA) muscle were stained with specific antibodies, HeyL was found in nearly all Pax7-positive nuclei, and Notch3 was expressed on the surface of mononuclear cells beneath the basal lamina (Fig. 2Cb, 2Cc). These results suggest that Notch3 and HeyL play roles in Notch signaling to inhibit muscle differentiation of satellite cells. Musculin/MyoR is a bHLH transcription factor originally cloned as a repressor of MyoD [33]. Musculin-null mice do not exhibit any skeletal muscle defect, but musculin is likely to negatively regulate MyoD in muscle regeneration [34].

In addition to negative regulators, two positive regulators of myogenesis, *Gli2* (*GLI-Kruppel family member GLI2*) (×29, ×13) and *Meox2* (*mesenchyme homeobox 2*) (×17), are preferentially expressed in quiescent satellite cells. Gli2 directly upregulates Myf5 [35], and Meox1 and 2 regulate Pax3 and Pax7 expressions [36]. These observations suggest that Gli2 and Meox2 maintain lineage identity in quiescent satellite cells.

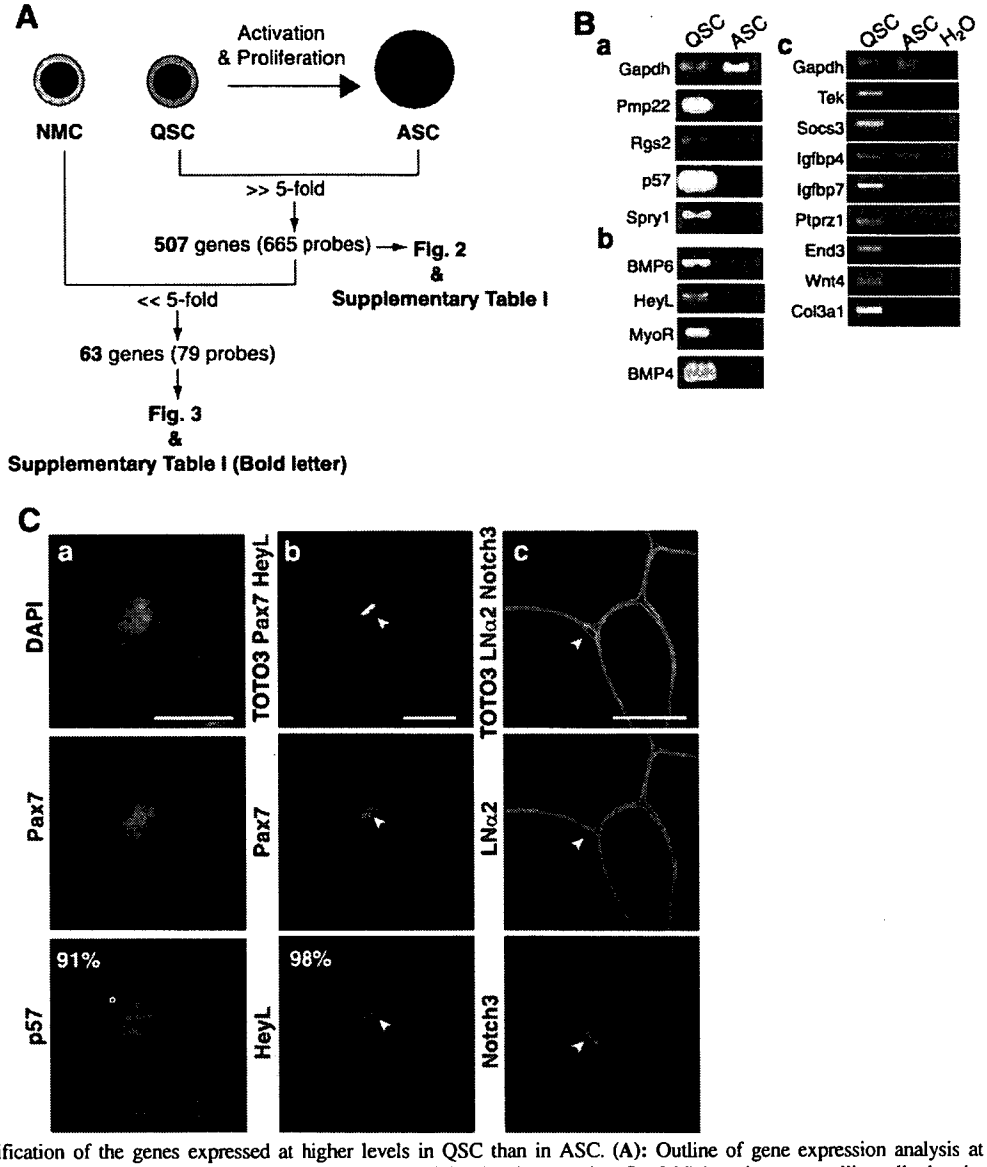


**Figure 2.** Identification of the genes expressed at higher levels in QSC than in ASC. **(A):** Outline of gene expression analysis at single gene level. Sixty-three genes out of 507 genes were found to be expressed at a higher level (more than fivefold) in quiescent satellite cells than in NMC. We applied Student's *t* test ($p$ value .05) with multiple testing corrections (Benjamini and Hochberg false discovery rate). **(B):** Reverse transcription-polymerase chain reaction of eight relevant genes involved in cell cycle regulation **(Ba)**, inhibition of myogenesis **(Bb)**, or other biological process **(Bc)** (Table 1). Total RNAs were isolated from fluorescence-activated cell sorting-sorted SM/C-2.6$^+$ cells (QSC) and cultured SM/C-2.6$^+$ cells (ASC). *Gapdh* is control. **(Ca):** Mononucleated cells from intact skeletal muscle were stained with anti-p57 (red), Pax7 (green), and DAPI (blue) immediately after sorting. **(Cb, Cc):** Cross-sections of normal skeletal muscle were stained with antibodies to HeyL (red in **[Cb]**), Notch3 (red in **[Cc]**), Pax7 (green in **[Cb]**), or laminin α2 chain (green in **[Cc]**). More than 90% of Pax7-positive cells were positive for p57. Nearly all Pax7-positive cells expressed HeyL. Notch3 was expressed on the cell surface on satellite cells. Nuclei were stained with TOTO3 (blue). Scale bar: 20 μm. Abbreviations: ASC, activated satellite cells; DAPI, 4,6-diamidino-2-phenylindole; LNα2, laminin α2; NMC, nonmyogenic cells; QSC, quiescent satellite cells.

## Identification of Quiescent Satellite Cell-Specific Genes

To identify quiescent satellite cell-specific genes from 507 genes (Fig. 2A), we next prepared RNA samples from nonmyogenic cells (SM/C-2.6$^-$/CD45$^-$ in Fig. 1A) and performed microarray analysis using Affymetrix GeneChips. Statistical analysis validated that 63 genes out of 507 genes were preferentially expressed (>fivefold) in quiescent satellite cells compared with nonmyogenic cells or activated satellite cells (genes in bold letters in supplemental online Table 1).

To confirm the microarray results, we next performed RT-PCR on 14 genes of interest. In addition to microarray samples, the results for TA muscle and a myogenic cell line, C2C12 cells, are also shown (Fig. 3). Two well-established satellite cell markers (Pax7 and M-cadherin) were expressed not only in quiescent satellite cells but also in activated satellite cells and/or C2C12 cells. In contrast, two cell surface molecules, Odz4, a mouse homolog of the *Drosophila* pair-rule gene *Odd Oz* [37], and CTR, a signaling molecule Tribbles1, and two extracellular molecules, endothelin3 and chordin-like2, were all confirmed to be expressed exclusively in quiescent satellite cells.

## Gene Set Enrichment Analysis Revealed Gene Groups Upregulated in Quiescent Satellite Cells

Single-gene analysis permitted us to identify candidate genes that regulate quiescence and undifferentiated state of satellite cells in vivo. To complement the analysis at the single gene

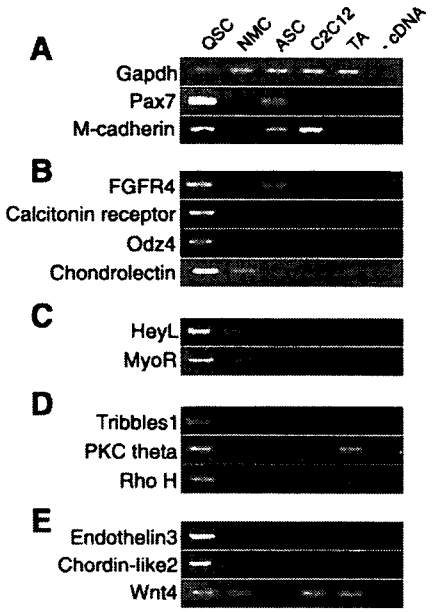


**Figure 3.** Reverse transcription-polymerase chain reaction (RT-PCR) of quiescent satellite cell-specific genes. Expression levels of quiescent satellite cell-specific genes in fluorescence-activated cell sorting-sorted SM/C-2.6$^+$ cells (lane 1), SM/C-2.6$^-$/CD45$^-$ nonmyogenic cells (lane 2), cultured SM/C-2.6$^+$ cells (lane 3), C2C12 cells (lane 4), and TA muscle (lane 5) were confirmed by RT-PCR. The genes are categorized into five groups: well-known satellite cell markers (**A**), cell surface receptors (**B**), transcription factors (**C**), signal molecules (**D**), and extracellular molecules (**E**). Lane 6 is the reaction without cDNA templates. Abbreviations: ASC, activated satellite cells; NMC, nonmyogenic cells; QSC, quiescent satellite cells; TA, tibialis anterior.

level, we performed gene set enrichment analysis [22]. GSEA is an analytical method that identifies small but coordinated changes of predefined gene sets but not up- or downregulation of individual genes, which therefore would help us to identify important signaling pathways or regulatory mechanisms for satellite cells. We used GO annotations [23] to group all genes on GeneChips and tried to extract gene sets that are upregulated as a whole in quiescent satellite cells compared with activated and proliferating satellite cells (Fig. 4). When all genes were categorized into 1,674 gene sets according to their biological process ontology, only three gene sets were judged to be coordinately upregulated in quiescent satellite cells (FDR $< 0.25$): cell-cell adhesion, regulation of cell growth, and transmembrane receptor protein tyrosine phosphatase signaling pathway (Table 1). When all genes were grouped into 1,698 gene sets according to cellular component ontology, three gene sets, insoluble fraction, extracellular region, and collagens, were found to be coordinately upregulated in quiescent satellite cells compared with activated/proliferating satellite cells (Table 1). When grouped into 412 gene sets based on their predicted molecular functions, three gene sets, extracellular matrix structural constituent conferring tensile strength, copper ion binding, and lipid transporter activity, were found to be coordinately upregulated in quiescent satellite cells (Table 1). Seven genes listed in Table 1 (*Tek, Socs3, Igfbp7, Ptprz1, End3, Wnt4,* and *Col3a1*) were confirmed to be upregulated in quiescent satellite cells by RT-PCR (Fig. 2Bc). A more detailed discussion on GSEA results is in the supplemental online Discussion.

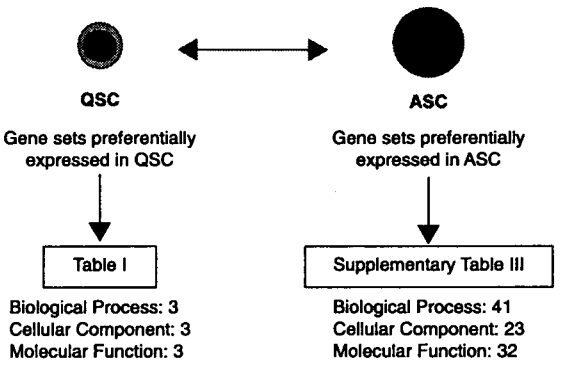


**Figure 4.** Gene set enrichment analysis (GSEA) of quiescent and activated satellite cells. Summary of GSEA comparing QSC with ASC using gene sets based on three major Gene Ontology trees: cellular component, biological process, and molecular function. Gene sets with high enrichment score (1 − [false discovery rate q value] are >0.75) are listed in Table 1 and supplemental online Table 3. Abbreviations: ASC, activated satellite cells; QSC, quiescent satellite cells.

## Gene Sets That Are Coordinately Upregulated upon Activation

Many gene sets were found to be coordinately upregulated in activated/proliferating satellite cells compared with quiescent satellite cells (Fig. 4). These are involved in active synthesis of DNA, RNA and protein, progression of cell cycle (*Cdc2a, Cdc20, Cdc25c, Ccnb1, Ccna2,* etc.), mitochondrial activities, and so on. The gene sets are all listed in supplemental online Table 3. The results well reflect active cell cycling and high metabolic activity of satellite cells.

## Expression of Cell-Cell Adhesion Molecules on Satellite Cells

Both single gene analysis and GSEA suggest that cell-cell adhesion is one of the key elements in the regulation of satellite cells. Preferential expression of the following genes in quiescent satellite cells was confirmed by RT-PCR and quantitative PCR (supplemental online Fig. 1A, 1B): *VE-cadherin* (*cadherin 5*), *Vcam1*, *Icam1*, *Cldn5* (*claudin 5*), *Esam* (*endothelial cell-specific adhesion molecule*), and *Pcdhb9* (*protocadherin beta 9*). To date, several cell surface markers for satellite cells have been identified, including M-cadherin, syndecan3, syndecan4, c-met, Vcam-1, NCAM-1, and CD34 [5, 38–43]. Vascular endothelial (VE)-cadherin, Icam1, claudin5, Esam, and Pcdhb9 should be added to the list. Because *Esam* is upregulated in long-term hematopoietic stem cells and mammary gland side population cells [44, 45], the expression of *Esam* in quiescent satellite cells is quite intriguing. When transverse sections of adult skeletal muscle were stained with specific antibodies, M-cadherin was found at the site of contact between satellite cells and myofibers (supplemental online Fig. 1C) [38]. Vcam-1 and VE-cadherin proteins are also detected at the boundary of satellite cells and myofibers. Although their roles in regulation of satellite cells remain to be determined, our observations suggest that cell-cell adhesion molecules have critical roles in keeping satellite cells in an undifferentiated and quiescent state and in protecting satellite cells from cell death. We also confirmed that FACS with Vcam-1 anti-

**Table 1.** Gene sets upregulated in quiescent satellite cells and genes with high enrichment scores

| | 1 − (FDR q value) |
|---|---|
| Biological process | |
| Cell-cell adhesion | .791 |
| *Tek, Vcam1, Icam2, Cldn5, Cdh5, Icam1* | |
| Regulation of cell growth | .787 |
| *Socs3, Htra1, Htra3, Ctgf, Igfbp4, Creg1, Igfbp7, Epc1, Cyr61, Crim1, Nov, Igfbp6, Nedd9* | |
| Transmembrane receptor protein tyrosine phosphatase signaling pathway | .751 |
| *Ptprz1, Ptprf, Ptprb, Ptprd, Ptprk, Ptprs, Ptprr* | |
| Cellular component | |
| Insoluble fraction | .786 |
| *Dmd, Dag1, Plec1, Des, Hspb1* | |
| Extracellular region | .766 |
| *Sepp1, Htra1, Edn3, Cxcl1, Loxl1, Htra3, Thbs4, Ctgf, Ntf3, Twsg1, Ccl27, Rarres2, Ltbp3, Igfbp4, Apoe, Igf1, Ibsp, Trf, Pthlh, Polydom, Ccl11, Abca3, Thbs3, Wnt4, Pros1, Vwa1, Comp, Nppc, Cyp4v3, Ccl19, Nts, Fbln2, Cocoacrisp, Cxcl2, Igfbp7, C1r, Thbs2, Ccl6, Calca, Cyr61, Icosl, Ccl21c, Crim1, Il6, Degb10, Cxcl9, Csng, C3, Cxcl10, Cxcl14, Inhbb, Il15, Nov, Igfbp6, Mglap, Dkk2, Tnfsf12, Ifnb1, Tfpi2, Cxcl11, Il18, Pi16, Pycard, Lzp-s, Stc1, Lyzs* | |
| Collagen | .766 |
| *Col3a1, Col6a2, Col17a1, Col1a2, Col15a1, Col6a3, Col5a3, Col1a1, Col4a1, Col5a1, Col11a1* | |
| Molecular function | |
| Extracellular matrix structural constituents conferring tensile strength | .774 |
| *Col3a1, Col6a2, Col17a1, Col1a2, Col15a1, Col6a3, Col16a1, Col1a1, Col4a1, Col4a5, Col5a1, Col11a1, Col11a2, Col9a1, Col4a2, Col4a4* | |
| Copper ion binding | .764 |
| *Aoc3, Cp, Loxl1, Mt1, Atp7a, Heph, Loxl2, Nr1h3* | |
| Lipid transporter activity | .752 |
| *Vldlr, Lpl, Apoe, Sorl1, Ldlr, Gpld1, Lrpl* | |

Gene names are listed according to the rank of enrichment scores. Underlined genes (46/118 genes) are also listed in supplemental online Table 1.
Abbreviation: FDR, false discovery rate.

body efficiently enriches quiescent satellite cells as SM/C-2.6 does (supplemental online Fig. 2).

## Calcitonin Receptor Is Sharply Downregulated on Activated Satellite Cells and Reappeared on Renewed Satellite Cells During Muscle Regeneration

RT-PCR verified that CTR is exclusively expressed in quiescent satellite cells but not in activated satellite cells or in nonmyogenic cells (Fig. 3). In addition, we confirmed that calcitonin mRNA is expressed in satellite cells (data not shown). Therefore, we examined the expression of CTR protein in vivo using immunohistochemistry. As shown in Figure 5A, CTR protein was observed in Pax7-positive mononuclear cells beneath the basal lamina in uninjured muscle. We next stained cross-sections of regenerating muscle with anti-CTR antibody. Three days after cardiotoxin injection, many activated satellite cells were stained with anti-M-cadherin antibodies, but CTR expression was not detected on activated satellite cells on the serial sections (Fig. 5B). Furthermore, there were no $Pax7^+/CTR^+$ cells on muscle sections until 7 days after injury (cardiotoxin [CTX]-7d), when $Pax7^+/CTR^+$ cells were again found at the periphery of centrally nucleated, relatively large myofibers but not of small regenerating fibers (Fig. 5C, 5D). The number of $Pax7^+/CTR^+$ cells gradually increased thereafter and reached the level of uninjured muscle by CTX-14d (Fig. 5D). Interestingly, approximately 20% of $Pax7^+/CTR^+$ cells on CTX-7d were found outside the basal lamina (Fig. 5E). This atypical position of satellite cells was transient, and the ratio of satellite cells residing beneath the basal lamina increased during myofiber maturation (data not shown). Taken together, the results suggest that the expression of CTR is found not only on quiescent satellite cells but also on newly formed satellite cells that are closely associated with maturing myofibers.

## Calcitonin Inhibits Activation of Quiescent Satellite Cells

To investigate the roles of CTR in the regulation of satellite cells, eel calcitonin, elcatonin, was added to the culture of quiescent satellite cells in vitro before or after activation. Addition of calcitonin before activation significantly inhibited BrdU uptake by quiescent satellite cells (Fig. 6A) but not by already activated satellite cells (Fig. 6A). Interestingly, a short exposure (0.5 hours) to calcitonin was enough to suppress the activation of quiescent satellite cells (Fig. 6B).

MyoD staining of satellite cells revealed that calcitonin/CTR signaling delays the induction of MyoD in quiescent satellite cells (Fig. 6C). The lower percentage of Ki67-positive cells in calcitonin-treated satellite cells also indicated that calcitonin delays the entry of quiescent satellite cells into the cell cycle (Fig. 6C). Calcitonin-treated cells were considerably smaller than control cells on the second day of culture (Fig. 6D), again indicating delayed activation of satellite cells in the presence of calcitonin. A terminal deoxynucleotidyl transferase dUTP nick-end labeling assay excludes the possibility that calcitonin induced apoptosis in satellite cells (Fig. 6E).

To further investigate the effects of calcitonin on activation of quiescent satellite cells, we prepared living single muscle fibers from mouse extensor digitorum longus muscles by using the collagenase digestion method [20] and plated them onto Matrigel-coated 24-well plates at a density of one fiber per well in the presence or absence of calcitonin. In control wells, many satellite cells had detached and migrated from the myofibers 2 days after plating (Fig. 6F). Calcitonin significantly reduced the numbers of satellite cells that had detached from myofibers (Fig. 6F). It was reported that

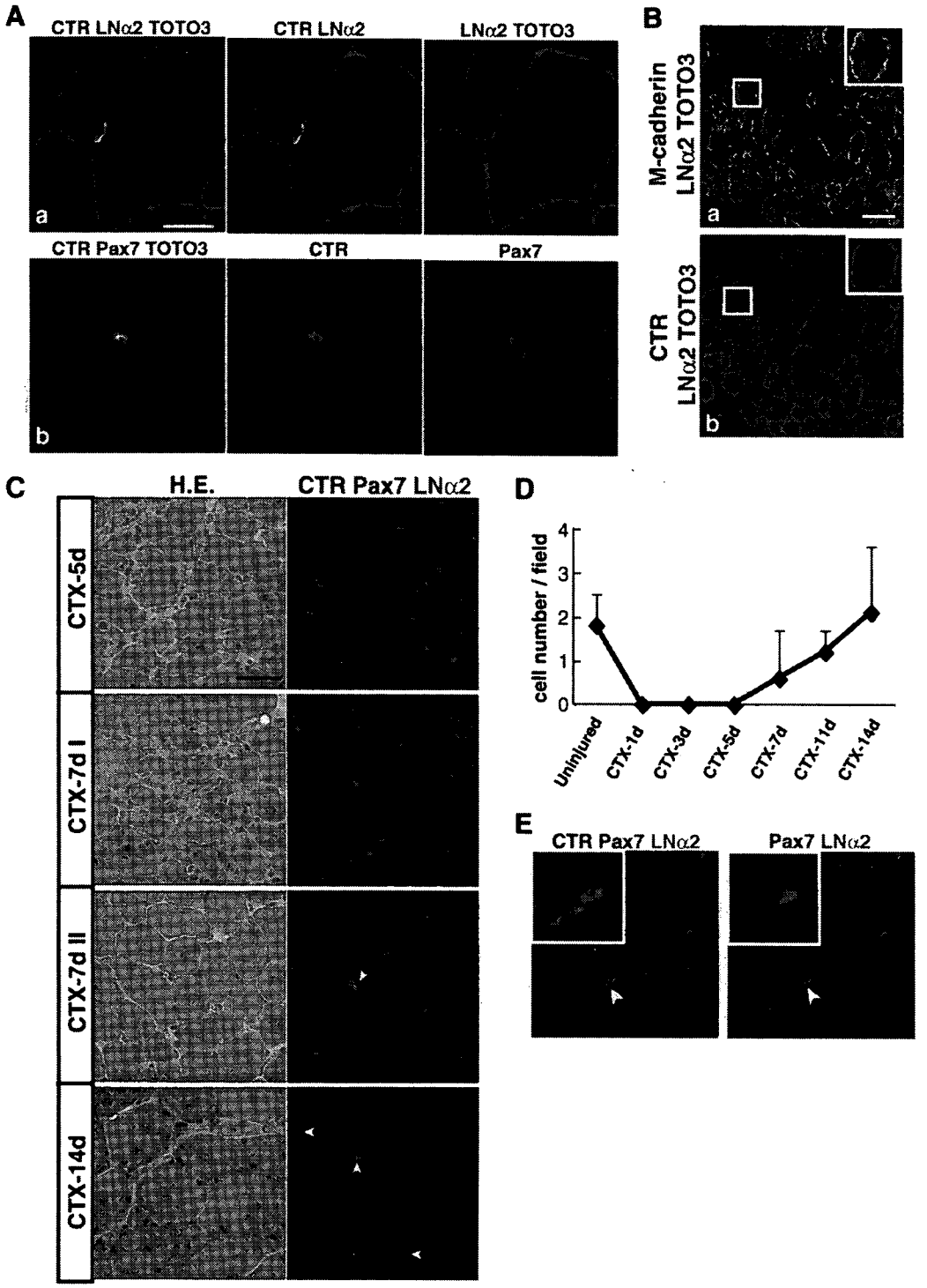


**Figure 5.** Reappearance of CTR- and Pax7-positive satellite cells in regenerating muscle 7 days after cardiotoxin injection. **(A):** Cross-sections of uninjured skeletal muscle were stained with antibodies to calcitonin receptor (red), laminin α2 chain (green in [Aa]), or Pax7 (green in [Ab]). Nuclei were stained with TOTO3 (blue). Scale bar: 20 μm. **(B):** Three days after CTX injection, regenerating muscles were dissected, and serial cross-sections were stained with antibodies to M-cadherin (red in **[Ba]**) or CTR (red in **[Bb]**) and anti-laminin α2 (green in **[Ba, Bb]**) antibodies. Insets show close-ups of marked areas by white squares. Nuclei were stained with TOTO3 (blue). Scale bar: 40 μm. **(C):** Tibialis anterior muscles were sampled at five (CTX-5d), seven (CTX-7d), and 14 days (CTX-14d) after CTX injection. Sections were coimmunostained with anti-CTR (red), Pax7 (green), and laminin α2 chain (blue) antibodies. Serial sections were stained with H.E. Note that $Pax7^+/CTR^+$ cells were first detected on the seventh day of regeneration around regenerating muscle fibers with a large diameter (CTX-7d II) but not around small-sized fibers (CTX-7d I). Arrowheads indicate CTR-positive Pax7-positive cells. Scale bar: 40 μm. **(D):** Numbers of $Pax7^+/CTR^+$ cells per field at 1, 3, 5, 7, 11, and 14 days after CTX injection. $Pax7^+/CTR^+$ cells were counted in 12–21 randomly selected fields in the regenerating area. The average is shown with SD. **(E):** Cross-sections of regenerating muscle 7 days after CTX injection were coimmunostained with CTR (red), Pax7 (green), and laminin α2 (blue). A typical $Pax7^+/CTR^+$ satellite cell outside the basal lamina is shown (arrowheads). Scale bar: 20 μm. Abbreviations: CTR, calcitonin receptor; CTX, cardiotoxin; d, day; H.E., hematoxylin and eosin; LNα2, laminin α2.

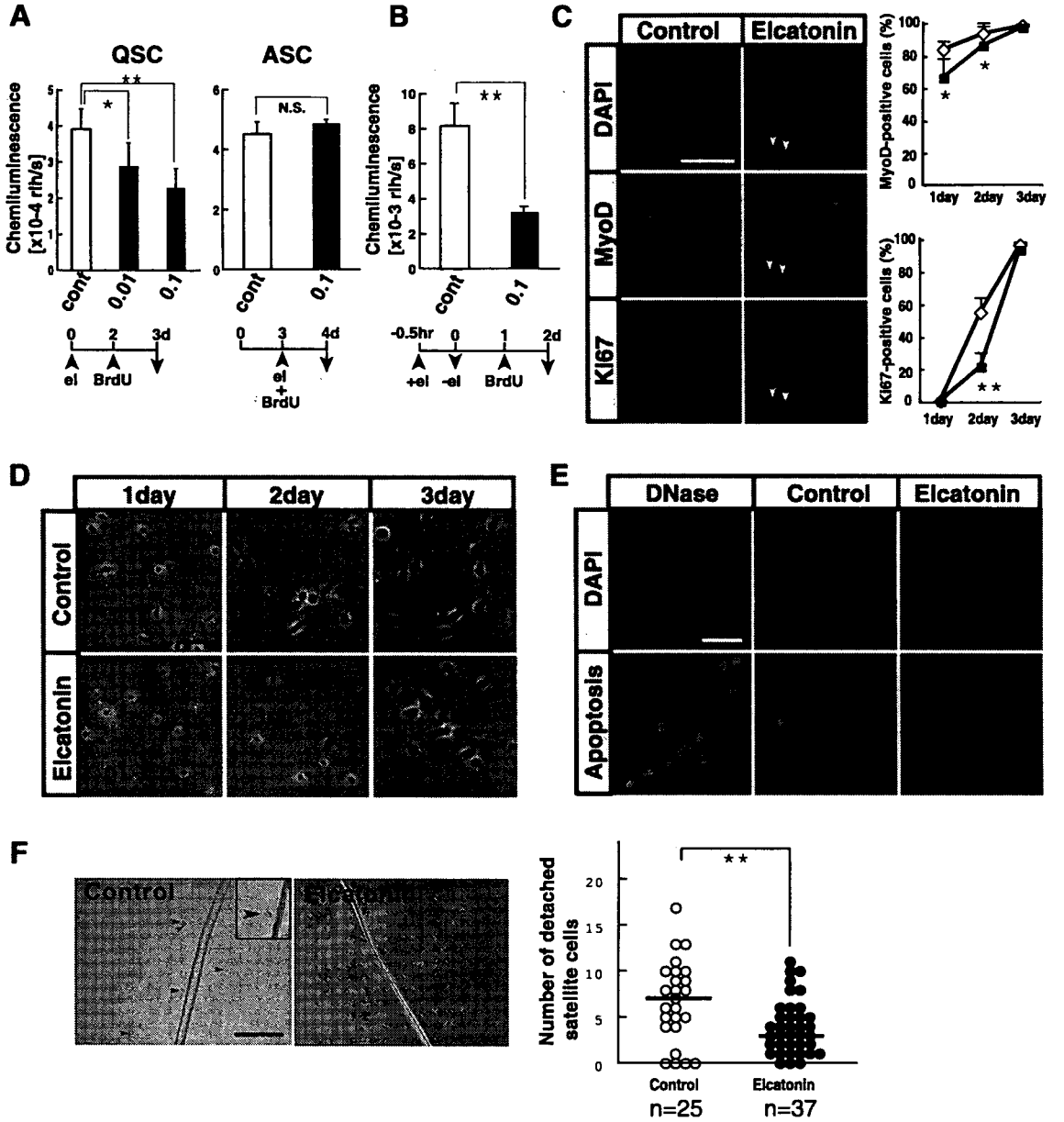


**Figure 6.** Calcitonin receptor agonist, elcatonin, suppresses activation of quiescent satellite cells. **(A):** Freshly isolated SM/C-2.6$^+$ cells (QSC) and cultured SM/C-2.6$^+$ cells (ASC) were grown in the presence (black) or absence (white) of eel calcitonin, elcatonin. Left: QSC were cultured for 2 days with (0.01 U/ml or 0.1 U/ml) or without elcatonin and then cultured for an additional 24 hours in the presence of BrdU. Right: QSC were cultured for 3 days and then cultured for 24 hours in the presence or absence of elcatonin and BrdU. The vertical axis shows the mean BrdU uptake by satellite cells of three experiments with SD; * $p < .05$, ** $p < .01$ (analysis of variance [ANOVA] test). **(B):** BrdU uptake by QSC exposed to elcatonin for 30 minutes prior to plating. Values are means with SD ($n = 3$); ** $p < .01$. **(C):** QSC cultured in the presence or absence of 0.1 U/ml elcatonin for 2 days were stained with anti-MyoD (red) or Ki67 (green) antibodies. Nuclei were stained with DAPI (blue). Arrowheads indicate MyoD- and Ki67-negative satellite cells. Graphs show the frequency of MyoD- or Ki67-positive cells 1, 2, or 3 days after plating with (closed square) or without (open diamond) elcatonin. More than 100 cells were counted. Values are means with SD; * $p < .05$, ** $p < .01$. Scale bar: 50 $\mu$m. **(D):** Phase contrast images of satellite cells 1, 2, and 3 days after plating in the presence or absence of 0.1 U/ml elcatonin. Note that many elcatonin-treated satellite cells are smaller than nontreated cells 2 days after plating. Scale bar: 50 $\mu$m. **(E):** Terminal deoxynucleotidyl transferase dUTP nick-end labeling assay on satellite cells cultured with or without elcatonin for 2 days. Apoptotic cells are in red. Nuclei were stained with DAPI (blue). As a positive control, satellite cells were pretreated with DNase. Scale bar: 50 $\mu$m. **(F):** Activation of satellite cells on myofibers in vitro. Isolated muscle fibers were plated at a density of one fiber per well and cultured with or without elcatonin (0.1 U/ml) for 2 days, and the numbers of satellite cells that had detached and migrated from each muscle fiber (arrowheads) were counted. Inset is a close-up image of a detached satellite cell. Scale bar: 100 $\mu$m. ANOVA $t$ test, ** $p < .01$. Abbreviations: ASC, activated satellite cells; BrdU, 5-bromo-2′-deoxyuridine; d, days; DAPI, 4,6-diamidino-2-phenylindole; el, elcatonin; hr, hours; NS, nonsignificant; QSC, quiescent satellite cells.

calcitonin signaling was mediated via cAMP [46]. An analog of cAMP, dibutyryl cAMP, and an activator of adenylate cyclase, forskolin, also attenuated the activation of satellite cells in vitro (data not shown). Collectively, our results suggest that calcitonin/CTR signaling inhibits activation of satellite cells but not their proliferation or survival. The downstream target molecules of calcitonin/CTR remain to be determined.

## CONCLUSION

Single gene-level analysis revealed several candidate genes that negatively regulate cell cycling of satellite cells. Furthermore, our results suggested that satellite cells express both myogenic and antimyogenic molecules to maintain their delicate state.

GSEA showed that dormant satellite cells coordinately express gene groups involved in cell-cell adhesion, cell-extracellular matrix interaction, copper and iron homeostasis, lipid transport, and regulation of cell growth. Although the result shows one aspect of regulation of quiescent satellite cells, more elaborate gene grouping might be needed to further understand the molecular regulation of quiescent satellite cells.

Finally, we showed that calcitonin receptor is specifically expressed on quiescent satellite cells and transmits signals that attenuate the entry of quiescent satellite cells into the cell cycle. Our results would greatly facilitate the investigation of molecular regulation of satellite cells in both physiological and pathological conditions.

## ACKNOWLEDGMENTS

This work was supported by Grants for Research on Nervous and Mental Disorders (16B-2), Health Science Research Grants for Research on the Human Genome and Gene Therapy (H16-genome-003), for Research on Brain Science (H15-Brain-021) from the Japanese Ministry of Health, Labor and Welfare, Grants-in-Aids for Scientific Research (14657158, 153,90281, and 165,90333) from the Japanese Ministry of Education, Culture, Sports, Science and Technology, and "Ground-Based Research Program for Space Utilization" promoted by Japan Space Forum.

## DISCLOSURE OF POTENTIAL CONFLICTS OF INTEREST

The authors indicate no potential conflicts of interest.

## REFERENCES

1 Bischoff R. Analysis of muscle regeneration using single myofibers in culture. Med Sci Sports Exerc 1989;21(suppl 5):S164–S172.
2 Partridge T. Reenthronement of the muscle satellite cell. Cell 2004;119: 447–448.
3 Mauro A. Satellite cell of skeletal muscle fibers. J Biophys Biochem Cytol 1961;9:493–495.
4 Schultz E, Gibson MC, Champion T. Satellite cells are mitotically quiescent in mature mouse muscle: an EM and radioautographic study. J Exp Zool 1978;206:451–456.
5 Cornelison DD, Wold BJ. Single-cell analysis of regulatory gene expression in quiescent and activated mouse skeletal muscle satellite cells. Dev Biol 1997;191:270–283.
6 Bischoff R. Satellite and stem cells in muscle regeneration. In: Engel AG, Franzini-Armstrong C, eds. Myology. Vol 1. New York: McGraw-Hill, 2004:66–86.
7 Collins CA, Olsen I, Zammit PS et al. Stem cell function, self-renewal, and behavioral heterogeneity of cells from the adult muscle satellite cell niche. Cell 2005;122:289–301.
8 Seale P, Sabourin LA, Girgis-Gabardo A et al. Pax7 is required for the specification of myogenic satellite cells. Cell 2000;102:777–786.
9 Grounds MD, Yablonka-Reuveni Z. Molecular and cell biology of skeletal muscle regeneration. Mol Cell Biol Hum Dis Ser 1993;3: 210–256.
10 Wagers AJ, Conboy IM. Cellular and molecular signatures of muscle regeneration: Current concepts and controversies in adult myogenesis. Cell 2005;122:659–667.
11 Asakura A, Komaki M, Rudnicki M. Muscle satellite cells are multipotential stem cells that exhibit myogenic, osteogenic, and adipogenic differentiation. Differentiation 2001;68:245–253.
12 Wada MR, Inagawa-Ogashiwa M, Shimizu S et al. Generation of different fates from multipotent muscle stem cells. Development 2002;129: 2987–2995.
13 Shefer G, Wleklinski-Lee M, Yablonka-Reuveni Z. Skeletal muscle satellite cells can spontaneously enter an alternative mesenchymal pathway. J Cell Sci 2004;117:5393–5404.
14 McCroskery S, Thomas M, Maxwell L et al. Myostatin negatively regulates satellite cell activation and self-renewal. J Cell Biol 2003;162: 1135–1147.
15 Thomas M, Langley B, Berry C et al. Myostatin, a negative regulator of muscle growth, functions by inhibiting myoblast proliferation. J Biol Chem 2000;275:40235–40243.
16 Cao Y, Zhao Z, Gruszczynska-Biegala J et al. Role of metalloprotease disintegrin ADAM12 in determination of quiescent reserve cells during myogenic differentiation in vitro. Mol Cell Biol 2003;23: 6725–6738.
17 Carnac G, Fajas L, L'Honore A et al. The retinoblastoma-like protein p130 is involved in the determination of reserve cells in differentiating myoblasts. Curr Biol 2000;10:543–546.
18 Fukada S, Higuchi S, Segawa M et al. Purification and cell-surface marker characterization of quiescent satellite cells from murine skeletal muscle by a novel monoclonal antibody. Exp Cell Res 2004;296: 245–255.
19 Uezumi A, Ojima K, Fukada S et al. Functional heterogeneity of side population cells in skeletal muscle. Biochem Biophys Res Commun 2006;341:864–873.
20 Rosenblatt JD, Lunt AI, Parry DJ et al. Culturing satellite cells from living single muscle fiber explants. In Vitro Cell Dev Biol Anim 1995; 31:773–779.
21 Ojima K, Uezumi A, Miyoshi H et al. Mac-1(low) early myeloid cells in the bone marrow-derived SP fraction migrate into injured skeletal muscle and participate in muscle regeneration. Biochem Biophys Res Commun 2004;321:1050–1061.
22 Mootha VK, Lindgren CM, Eriksson KF et al. PGC-1alpha-responsive genes involved in oxidative phosphorylation are coordinately downregulated in human diabetes. Nat Genet 2003;34:267–273.
23 Ashburner M, Ball CA, Blake JA et al. Gene ontology: Tool for the unification of biology. The Gene Ontology Consortium. Nat Genet 2000;25:25–29.
24 Holyoake T, Jiang X, Eaves C et al. Isolation of a highly quiescent subpopulation of primitive leukemic cells in chronic myeloid leukemia. Blood 1999;94:2056–2064.
25 Missero C, Calautti E, Eckner R et al. Involvement of the cell-cycle inhibitor Cip1/WAF1 and the E1A-associated p300 protein in terminal differentiation. Proc Natl Acad Sci U S A 1995;92:5451–5455.
26 Zhang P, Wong C, Liu D et al. p21(CIP1) and p57(KIP2) control muscle differentiation at the myogenin step. Genes Dev 1999;13:213–224.
27 Cooper RN, Tajbakhsh S, Mouly V et al. In vivo satellite cell activation via Myf5 and MyoD in regenerating mouse skeletal muscle. J Cell Sci 1999;112:2895–2901.
28 Reshef R, Maroto M, Lassar AB. Regulation of dorsal somitic cell fates: BMPs and Noggin control the timing and pattern of myogenic regulator expression. Genes Dev 1998;12:290–303.
29 Dahlqvist C, Blokzijl A, Chapman G et al. Functional Notch signaling is required for BMP4-induced inhibition of myogenic differentiation. Development 2003;130:6089–6099.
30 Kuroda K, Tani S, Tamura K et al. Delta-induced Notch signaling mediated by RBP-J inhibits MyoD expression and myogenesis. J Biol Chem 1999;274:7238–7244.
31 Conboy IM, Rando TA. The regulation of Notch signaling controls satellite cell activation and cell fate determination in postnatal myogenesis. Dev Cell 2002;3:397–409.
32 Conboy IM, Conboy MJ, Smythe GM et al. Notch-mediated restoration of regenerative potential to aged muscle. Science 2003;302: 1575–1577.
33 Lu J, Webb R, Richardson JA et al. MyoR: A muscle-restricted basic helix-loop-helix transcription factor that antagonizes the actions of MyoD. Proc Natl Acad Sci U S A 1999;96:552–557.
34 Zhao P, Hoffman EP. Musculin isoforms and repression of MyoD in muscle regeneration. Biochem Biophys Res Commun 2006;342: 835–842.
35 Gustafsson MK, Pan H, Pinney DF et al. Myf5 is a direct target of long-range Shh signaling and Gli regulation for muscle specification. Genes Dev 2002;16:114–126.
36 Mankoo BS, Skuntz S, Harrigan I et al. The concerted action of Meox homeobox genes is required upstream of genetic pathways essential for the formation, patterning and differentiation of somites. Development 2003;130:4655–4664.

37 Zhou XH, Brandau O, Feng K et al. The murine Ten-m/Odz genes show distinct but overlapping expression patterns during development and in adult brain. Gene Expr Patterns 2003;3:397–405.
38 Irintchev A, Zeschnigk M, Starzinski-Powitz A et al. Expression pattern of M-cadherin in normal, denervated, and regenerating mouse muscles. Dev Dyn 1994;199:326–337.
39 Cornelison DD, Filla MS, Stanley HM et al. Syndecan-3 and syndecan-4 specifically mark skeletal muscle satellite cells and are implicated in satellite cell maintenance and muscle regeneration. Dev Biol 2001;239: 79–94.
40 Beauchamp JR, Heslop L, Yu DS et al. Expression of CD34 and Myf5 defines the majority of quiescent adult skeletal muscle satellite cells. J Cell Biol 2000;151:1221–1234.
41 Jesse TL, LaChance R, Iademarco MF et al. Interferon regulatory factor-2 is a transcriptional activator in muscle where It regulates expression of vascular cell adhesion molecule-1. J Cell Biol 1998; 140:1265–1276.
42 Illa I, Leon-Monzon M, Dalakas MC. Regenerating and denervated human muscle fibers and satellite cells express neural cell adhesion molecule recognized by monoclonal antibodies to natural killer cells. Ann Neurol 1992;31:46–52.
43 Charge SB, Rudnicki MA. Cellular and molecular regulation of muscle regeneration. Physiol Rev 2004;84:209–238.
44 Forsberg EC, Prohaska SS, Katzman S et al. Differential expression of novel potential regulators in hematopoietic stem cells. PLoS Genet 2005;1:e28.
45 Behbod F, Xian W, Shaw CA et al. Transcriptional profiling of mammary gland side population cells. STEM CELLS 2006;24:1065–1074.
46 Becker K, Muller B, Nylen E et al. Calcitonin Gene Family of Peptides. Vol 1. 2nd ed. New York: Academic Press, 2002.

See www.StemCells.com for supplemental material available online.

Gene Therapy (2007) 14, 1249–1260

www.nature.com/gt

ORIGINAL ARTICLE

# Injection of a recombinant AAV serotype 2 into canine skeletal muscles evokes strong immune responses against transgene products

K Yuasa[1,2], M Yoshimura[1], N Urasawa[1], S Ohshima[1], JM Howell[3], A Nakamura[1], T Hijikata[2], Y Miyagoe-Suzuki[1] and S Takeda[1]

[1]*Department of Molecular Therapy, National Institute of Neuroscience, National Center of Neurology and Psychiatry, Kodaira, Tokyo, Japan;* [2]*Research Institute of Pharmaceutical Sciences, Faculty of Pharmacy, Musashino University, Nishi-tokyo, Tokyo, Japan and* [3]*Division of Veterinary and Biomedical Sciences, Murdoch University, Perth, Western Australia, Australia*

*Using murine models, we have previously demonstrated that recombinant adeno-associated virus (rAAV)-mediated microdystrophin gene transfer is a promising approach to treatment of Duchenne muscular dystrophy (DMD). To examine further therapeutic effects and the safety issue of rAAV-mediated microdystrophin gene transfer using larger animal models, such as dystrophic dog models, we first investigated transduction efficiency of rAAV in wild-type canine muscle cells, and found that rAAV2 encoding β-galactosidase effectively transduces canine primary myotubes* in vitro. *Subsequent rAAV2 transfer into skeletal muscles of normal dogs, however, resulted in low and transient expression of β-galactosidase together with intense cellular infiltrations* in vivo, *where cellular and humoral immune responses were remarkably activated. In contrast, rAAV2 expressing no transgene elicited no cellular infiltrations. Co-administration of immunosuppressants, cyclosporine and mycophenolate mofetil could partially improve rAAV2 transduction. Collectively, these results suggest that immune responses against the transgene product caused cellular infiltration and eliminated transduced myofibers in dogs. Furthermore,* in vitro *interferon-γ release assay showed that canine splenocytes respond to immunogens or mitogens more susceptibly than murine ones. Our results emphasize the importance to scrutinize the immune responses to AAV vectors in larger animal models before applying rAAV-mediated gene therapy to DMD patients.*

Gene Therapy (2007) **14**, 1249–1260; doi:10.1038/sj.gt.3302984; published online 21 June 2007

**Keywords:** *AAV; gene transfer; skeletal muscle; dog; immune response; Duchenne muscular dystrophy*

## Introduction

Duchenne muscular dystrophy (DMD) is an X-linked, lethal disorder of skeletal muscle caused by mutations in the dystrophin gene, which encodes a large subsarcolemmal cytoskeletal protein, dystrophin. DMD is characterized by a high incidence (one among 3500 boys) and a high frequency of *de novo* mutation.[1] The absence of dystrophin accompanies the loss of dystrophin-associated glycoprotein complex from the sarcolemma and results in progressive muscle weakness, cardiomyopathy and early death. Although several treatment modalities, such as gene, cell and pharmacological therapies, have been researched to aim at correcting the dystrophic phenotypes, DMD currently has no effective treatment.

An adeno-associated virus (AAV) vector is a potential tool for gene therapy of inherited neuromuscular disorders. It is a nonpathogenic, low immunogenic and replication-defective viral vector that effectively infect nondividing cells, such as skeletal muscle fibers.[2] The size of exogenous DNA fragment which can be inserted into recombinant AAV vectors (rAAVs), however, is limited to up to 4.9 kb. Therefore, full-length dystrophin (14 kb) and mini-dystrophin (6.4 kb) cDNAs are too large to be incorporated into a rAAV. We and others have tried to design a short but functional microdystrophin gene that could be utilized as the therapeutic tool for DMD.[3–6] We constructed a series of rod-truncated microdystrophin cDNAs,[3] and generated transgenic *mdx* mice expressing each microdystrophin, and demonstrated that microdystrophin CS1 with four rod repeats and three hinges was a good candidate for therapeutic molecule.[7] We have also showed that the muscle-specific muscle creatine kinase (MCK) promoter in a rAAV drives longer transgene expression than the ubiquitous cytomegalovirus (CMV) promoter in *mdx* muscle.[8] Therefore, we generated the rAAV2 expressing microdystrophin ΔCS1 (3.8 kb cDNA) driven by the MCK promoter and introduced it into *mdx* muscles, and showed that sustained expression of microdystrophin from rAAV significantly ameliorates dystrophic phenotypes of

Correspondence: Dr S Takeda, Department of Molecular Therapy, National Institute of Neuroscience, National Center of Neurology and Psychiatry, 4-1-1 Ogawa-higashi, Kodaira, Tokyo 187-8502, Japan.
E-mail: takeda@ncnp.go.jp
Received 8 October 2006; revised 3 April 2007; accepted 14 May 2007; published online 21 June 2007

treated *mdx* mice.[9] These results indicate that rAAV-mediated microdystrophin transfer is a good therapeutic strategy for dystrophin deficiency.

For the application of our strategy to DMD patients, it is necessary to examine the therapeutic effects and the safety issue in larger animal models. To this end, we have recently established a colony of beagle-based canine X-linked muscular dystrophy in Japan ($CXMD_J$).[10,11] In contrast to moderate dystrophic changes of *mdx* mice, $CXMD_J$ show similar dystrophic phenotypes to those of human DMD: increased serum creatine kinase level, gross muscle atrophy with joint contractures, cardiomyopathy, prominent muscle necrosis, degeneration with mineralization and concurrent regeneration, and endomysial and perimysial fibrosis.[11,12] Therefore, affected dogs are useful for preclinical trials to predict the clinical effectiveness in DMD application. In addition, side effects of treatment modalities should be investigated in detail in the dog model to avoid unexpected, detrimental effects on DMD patients. For instance, human trial in hemophilia B was ineffective due to T-cell-mediated immunity to AAV capsid antigens, and represented the matter that further studies for immunomodulation in preclinical and human trials were required to achieve successful transduction.[13]

In this report, we demonstrate that rAAV2 efficiently infect canine myotubes and express the *lacZ* gene *in vitro*. In contrast, rAAV-mediated gene transfer into canine muscle *in vivo* elicits severe immune responses against the gene product, due to susceptive immune responses in the dog. These results suggest that it is important to know molecular backgrounds of immune response against AAV particles and its gene product in the host and consider immunosuppression in preclinical and clinical settings.

## Results

### *rAAV2-CMVLacZ efficiently transduces canine primary myotubes* in vitro

To investigate the transduction efficiency of a rAAV2 in canine muscle cells, we first infected primary myotubes prepared from C57BL/6 mice and wild-type beagle with rAAV type 2 encoding β-galactosidase (β-gal) driven by the CMV promoter (rAAV2-CMVLacZ) at doses from $2 \times 10^8$ to $2 \times 10^{11}$ vector genomes (vg) (Figure 1). Surprisingly, more canine myotubes were β-gal-positive than murine ones. To enhance the transgene expression by converting single-strand viral DNAs into double-strand DNAs after the rAAV infection,[14] we next co-infected myotubes with helper adenovirus (Ad) and rAAV2. As expected, Ad enhanced the expression of *lacZ* in both murine and canine myotubes, but β-gal expression was much more robust in canine primary myotubes than in mouse primary myotubes.

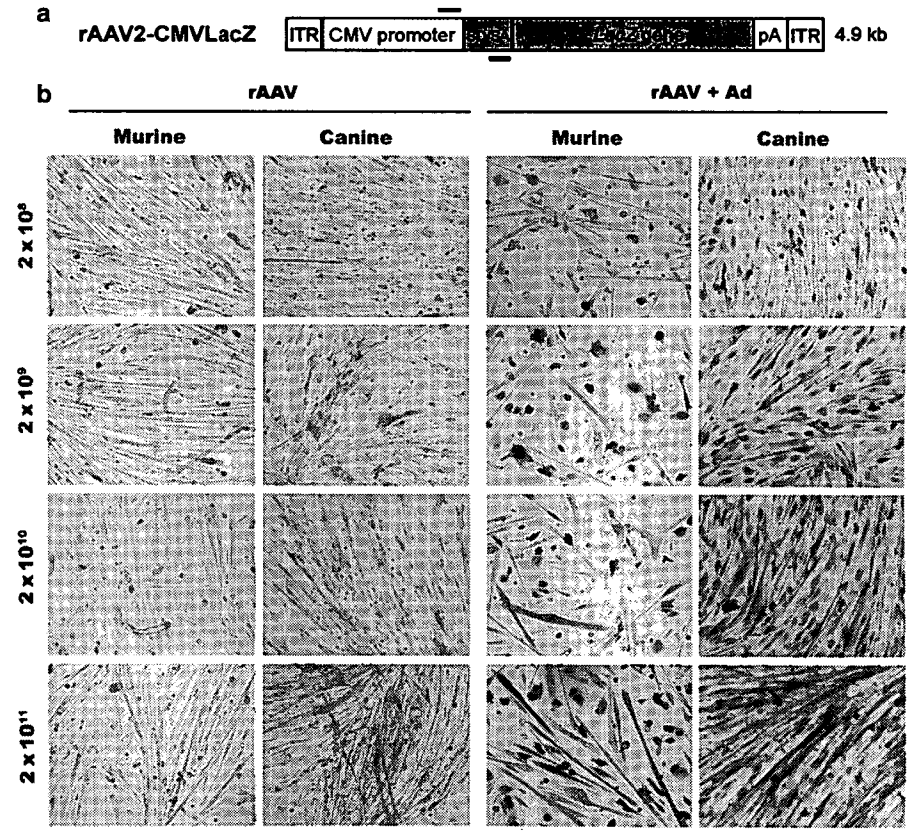


**Figure 1** Successful transduction of a rAAV2 in murine or canine primary myotubes *in vitro*. (a) Diagram of rAAV2-CMVLacZ. Upper and lower bars correspond to primer positions used for detection of genome and mRNA in Figure 2b. SD/SA: splicing donor and acceptor. (b) *In vitro* infection assay of rAAV2-CMVLacZ in murine and canine primary myotubes. Myotubes were infected with serial doses ($2 \times 10^8$–$2 \times 10^{11}$ vg/well) of rAAV2-CMVLacZ in the absence or presence of adenovirus (+Ad), and 2 days later β-gal expression was detected by X-Gal staining. Magnification: × 400. β-gal, β-galactosidase; X-Gal, 5-bromo-4-chloro-3-indolyl-β-D-galactopyranoside.

### *Low efficacy of gene transfer via rAAV into canine skeletal muscle* in vivo

To examine the transduction efficiency of rAAV2 in canine myofibers *in vivo*, rAAV2-CMVLacZ was injected into skeletal muscles of wild-type beagles and golden retrievers at various ages, and β-gal expression in the rAAV-injected muscles were evaluated at 2, 4 and 8 weeks after the injection (Figure 2a and Table 1). We previously reported that intramuscular injection of the rAAV2 into normal mice permitted sustained β-gal expression for at least 8 weeks.[8] In contrast to the mice, however, a few β-gal-positive fibers were observed in canine muscles at 2, 4 and 8 weeks after the injection of rAAV2-CMVLacZ both in beagles and golden retrievers. Moreover, in the rAAV2-injected canine muscles, a large number of mononuclear cells were observed around β-gal-expressing fibers at 2, 4 and 8 weeks after the injection (hematoxylin and eosin (H&E) in Figure 2a, Table 1). rAAV injection at neonatal stage or administration of low dose of the rAAV resulted in a little prolonged

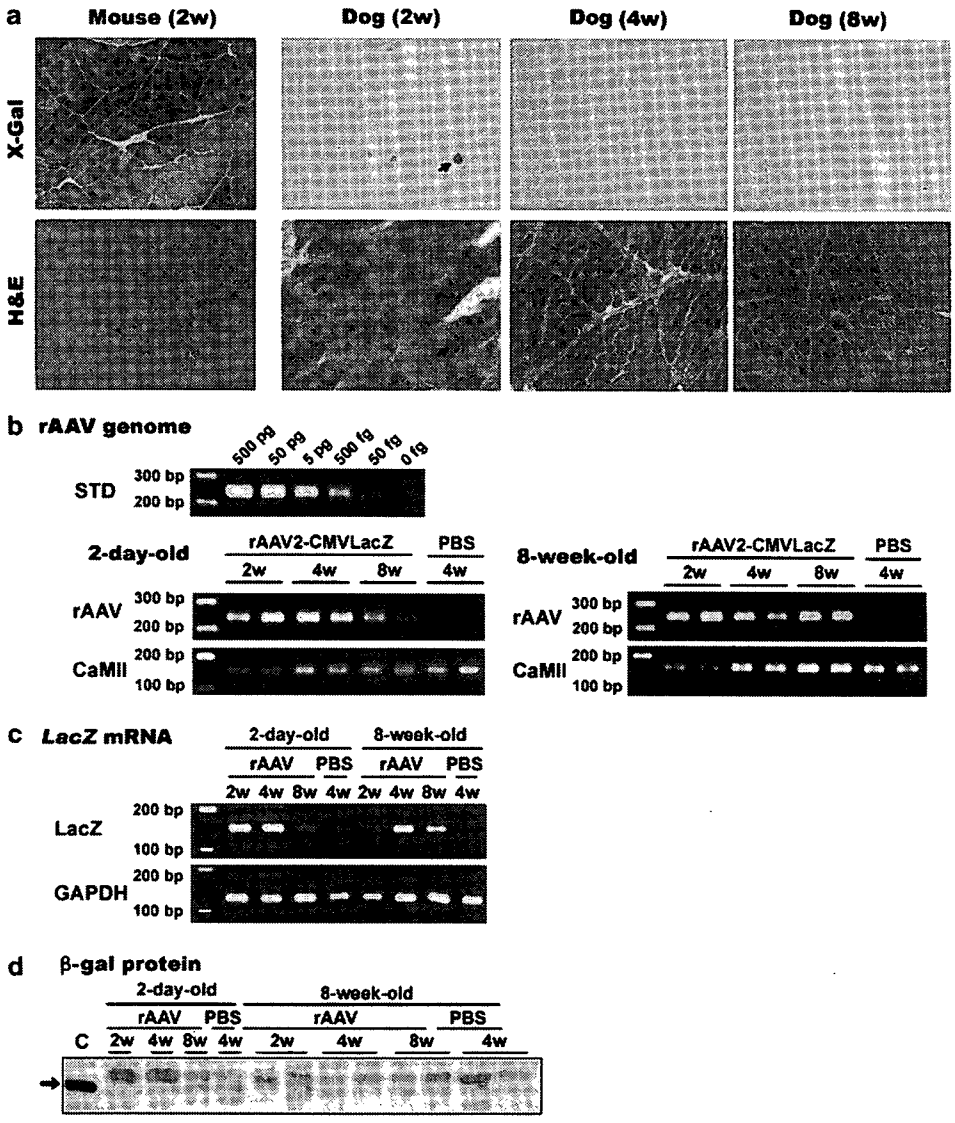


**Figure 2** Low transgene expression and marked cellular infiltration after rAAV2-mediated gene transfer into canine skeletal muscle. rAAV2-CMVLacZ was injected into normal muscles of beagles or golden retrievers at various ages. (**a**) Representative images of β-gal expression and histological change in the rAAV-injected murine (TA) and canine muscles at 2, 4 and 8 weeks post-injection (left TA, right TA and right ECU muscles of dog FD89 in Table 1, respectively). The same batches of rAAV2-CMVLacZ were injected into murine and canine skeletal muscles. Identical parts of the serial cross-sections were shown in X-Gal and H&E stains. Large and widespread (2w), or scattered clusters (4w, 8w) of infiltrating cells were observed in the rAAV-injected canine muscles. Magnification: × 200. (**b**, **c** and **d**) Detection of rAAV genomes (**b**), transgene mRNA (**c**) and β-gal protein (**d**) in the canine muscles injected at 2 days (dogs: 3290 and 0665) and 8 weeks (dogs: 0338). Total DNA, RNA or protein was extracted from rAAV2-CMVLacZ- or PBS-injected muscles after 2, 4 and 8 weeks post-injection. Genome (244 bp) or mRNA sequences (178 bp) of the rAAV was amplified from 200 ng of template DNA or an aliquot of RNA by PCR or RT-PCR, respectively (**b**, **c**). STD: quantity standard of AAV vector plasmid; rAAV: rAAV2-CMVLacZ genome; LacZ: β-gal mRNA; CaMII and GAPDH: internal controls of genome and message. Muscle extracts (40 μg/lane) and control β-gal (lane c) were separated on a sodium dodecyl sulphate-polyacrylamide gel, and β-gal (arrow) was detected by western blotting (**d**). AAV, adeno-associated virus; β-gal, β-galactosidase; GAPDH, glyceraldehyde-3-phosphate dehydrogenase; H&E, hematoxylin and eosin; rAAV, recombinant adeno-associated virus; TA, tibialis anterior.

**Table 1** Gene transfer of rAAV2-CMVLacZ into canine skeletal muscles

| *Animal*[a] | | | *Injection*[b] | β-*Gal expression*[c] | | | *Cellular infiltration*[d] | | |
|---|---|---|---|---|---|---|---|---|---|
| | | | | *2 weeks* | *4 weeks* | *8 weeks* | *2 weeks* | *4 weeks* | *8 weeks* |
| *Injection at 2 days* | | | | 10 days | 30 days | 65 days | 10 days | 30 days | 65 days |
| 9223 | GR | F | ($8.2 \times 10^{11}$ vg/100 μl) | ± | − | − | ± | ± | ± |
| 3290 | B | M | ($1.5 \times 10^{12}$ vg/100 μl) | − | ± | − | + | ++ | + |
| 7690 | B | M | ($1.5 \times 10^{12}$ vg/100 μl) | ± | ± | − | + | ++ | ± |
| 0665 | B | M | ($2.2 \times 10^{12}$ vg/100 μl) | ± | − | − | + | ++ | ± |
| *Injection at 4 weeks* | | | | 13d | | | 13d | | |
| 7329 | B | F | ($1.0 \times 10^{12}$ vg/100 μl) | −, −, −, − | | | +, +, +, + | | |
| 4657 | B | F | ($1.0 \times 10^{12}$ vg/100 μl) | ±, − | | | +, ± | | |
| *Injection at 8 weeks* | | | | 10 days | 30 days | 59 days | 10 days | 30 days | 59 days |
| 02490 | B | M | ($5.0 \times 10^{12}$ vg/500 μl) | | −, −, − | | | ++, ++, + | |
| 0338 | GR | M | ($8.0 \times 10^{12}$ vg/500 μl) | ++ | − | − | + | ++ | + |
| FD89 | GR | F | ($8.0 \times 10^{12}$ vg/500 μl) | ± | − | − | ++ | + | + |
| *Injection at 10 weeks* | | | | 14 days | 28 days | | 14 days | 28 days | |
| 901[e] | B | M | ($5.0 \times 10^{10}$ vg/500 μl) | ± | ± | | − | + | |
| | | | ($5.0 \times 10^{11}$ vg/500 μl) | − | ± | | − | ++ | |
| *Injection at 12 weeks* | | | | 10 days | 30 days | 59 days | 10 days | 30 days | 59 days |
| FF04 | GR | M | ($8.0 \times 10^{12}$ vg/500 μl) | ± | − | − | ++ | + | ± |
| E566 | GR | M | ($8.0 \times 10^{12}$ vg/500 μl) | − | − | − | ++ | + | − |
| *Injection at 16 weeks* | | | | | 27 days | | | 27 days | |
| 02232 | B | M | ($5.0 \times 10^{12}$ vg/500 μl) | | −, −, − | | | ++, +, + | |
| *Injection at 6 months* | | | | 14 days | | | 14 days | | |
| 0065 | B | F | ($7.5 \times 10^{12}$ vg/500 μl) | ± | | | + | | |
| *Injection at 14 months* | | | | | 28 days | | | 28 days | |
| D01 | B | M | ($5.0 \times 10^{11}$ vg/500 μl) | | −, −, − | | | +, ±, + | |
| D03 | B | M | ($5.0 \times 10^{12}$ vg/500 μl) | | −, −, − | | | +, ++, ++ | |

[a]Canine species and sex: B, beagle; GR, golden retriever; M, male; F, female.
[b]Dosage per muscle: rAAV titer (vg) and injection volume (μl).
[c]β-Gal-positive fibers: −, 0; ±, <100; +, <300; ++, <1000; +++, >1000.
[d]Infiltrating cells: −, not detected; ±, few; +, moderate; ++, extensive.
[e]Two kinds of dosages of rAAV were injected into a dog.
In [c] and [d], individual results of the injected muscles were shown.

expression of the transferred gene (Table 1, dogs 3290, 7690 and 901). To determine whether contamination of cellular proteins in the stocks of AAV vectors lowers transduction efficiency, we tried three different AAV preparation protocols: (i) two-cycle CsCl density gradient ultracentrifugation, (ii) heparin column chromatography, or (iii) combination of them, and found that preparation using heparin column chromatography showed high levels of contamination of transgene products and cellular proteins (Supplementary Figure 1). CsCl ultracentrifugation efficiently eliminated contaminated empty viral particles. Combination of these two methods almost completely eliminated contaminated proteins. Nevertheless, all rAAV stocks showed high levels of β-gal expression in murine muscles (data not shown), but evoked cellular infiltration in normal canine muscles (Supplementary Figure 1).

To quantify the levels of infection and transduction of rAAV2-CMVLacZ in canine muscles, we isolated DNA and RNA from the injected muscles, and semiquantitatively evaluated rAAV genome copy numbers and the level of β-gal mRNA by PCR and reverse transcription (RT)-PCR, respectively. AAV vector genomes and β-gal mRNA were detected at 2, 4 and 8 weeks after the injection (Figures 2b and c). β-Gal protein, however, could not be detected by western blot at all stages after the injection (Figure 2d). These results suggest that canine myofibers were transduced by a rAAV2 *in vivo*, but the transduced cells were eliminated by the host's defense mechanisms.

### *rAAV-mediated gene transfer into canine muscles evoke both cellular and humoral immune response*

We next analyzed cell markers on infiltrating cells in the rAAV2-CMVLacZ-injected muscles (Figure 3a) at 2 weeks after the injection at 12 weeks. Numerous CD4+ or CD8+ T lymphocytes were detected in the interstitial spaces of the injected muscle. CD11b+ cells and B cells were also detected in the cluster of infiltrating cells. Furthermore, the expression of the major histocompatibility complex (MHC) class I and -II molecules were highly upregulated on both mononuclear cells and muscle fibers. IgG deposits were found in both the

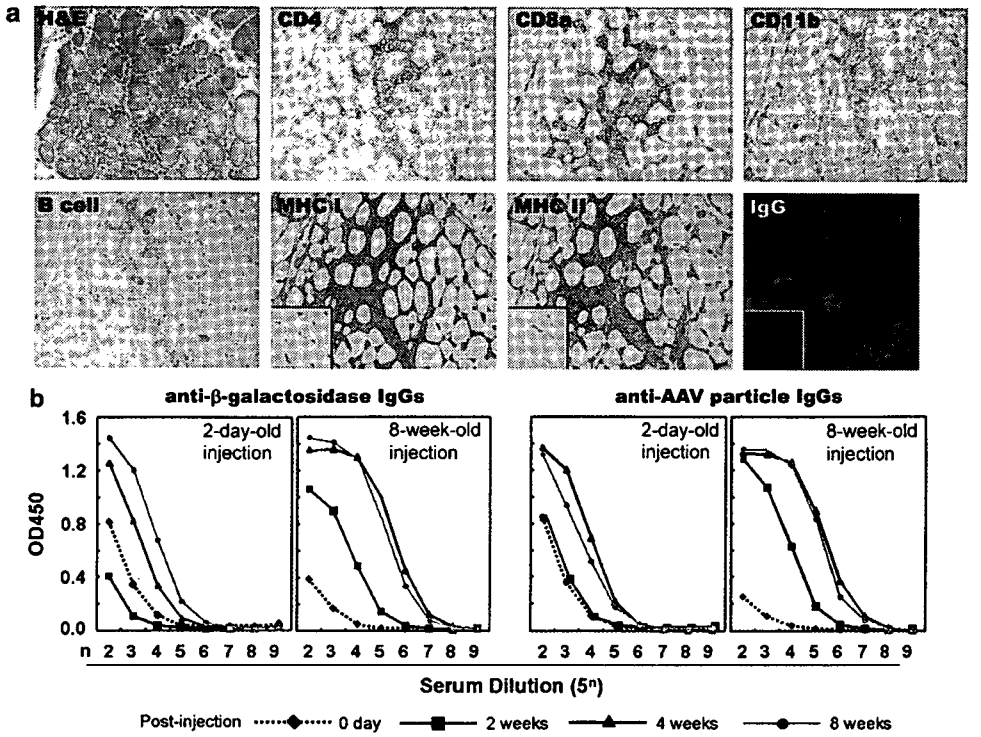


**Figure 3** Immune responses were remarkably activated after rAAV2-mediated gene transfer into canine muscles. (a) Infiltrating cells in the rAAV2-CMVLacZ-injected canine TA muscles at 2 weeks after the injection. Serial cross-sections were immunostained with antibodies against canine CD4, CD8a, CD11b, B cell, MHC class I and -II, and IgGs. Insets show the noninjected muscles. Dog: FF04. Magnification: ×400. (b) Humoral immune responses against the transgene product and rAAV particle in the rAAV-treated dogs. Sera from dogs injected with rAAV2-CMVLacZ at 2 days and 8 weeks were analyzed for the presence of IgG antibodies against β-gal or AAV particle at 0, 2, 4 and 8 weeks after the injection, using ELISA. Dogs: 9223 and 0338. AAV, adeno-associated virus; β-gal, β-galactosidase; ELISA, enzyme-linked immunosorbent assay; MHC, major histocompatibility complex; rAAV, recombinant adeno-associated virus; TA, tibialis anterior.

cytoplasm of myofibers and the extracellular space in the rAAV-injected muscle. We next examined the antibodies against the transgene product or rAAV particles in the sera of rAAV-injected dogs (Figure 3b). The levels of serum IgGs that react β-gal protein or rAAV2 particle were gradually increased with time in both 2-day-old and 8-week-old injections. When injected at 8 weeks, the levels of IgGs against β-gal or rAAV2 increased from 2 weeks after the injection, and reached the peak at 4 weeks. When injected at 2 days, anti-β-gal or anti-AAV antibodies were not detected at 2 weeks after the injection, but had begun to increase at 4 weeks. The results would explain why the lacZ was expressed for a longer time, when injected at neonatal age (Table 1). These results suggest that cellular and humoral immune responses are elicited after the transfer of a rAAV2 into canine muscles.

### *Administration of a rAAV expressing no transgene into canine muscles*

Transduction of skeletal muscle by rAAV2-CMVLacZ presents two main foreign antigens, namely β-gal protein and AAV capsid to the host's immune system. To test which antigen is responsible for rapid elimination of transduced myofibers after rAAV-mediated gene transfer into canine muscle, we constructed a rAAV2 expressing no transgene, named rAAV2-LacZ-P(−), by removing the MCK promoter from the parental rAAV2-MCKLacZ (Figure 4a). We confirmed that the promoter-deleted rAAV2 expressed no β-gal in muscle after injection into skeletal muscles of normal mice ($5 \times 10^{11}$ vg/50 μl/site) (data not shown). Then, we injected the same titers of rAAV2-LacZ-P(−) and rAAV2-CMVLacZ, into skeletal muscles of normal adult beagles, and evaluated transduction efficiency by quantitative PCR of AAV genomes or histopathologically at 2 and 4 weeks post-injection. In 5 × 5 × 10 mm tissues of rAAV2-LacZ-P(−)-injected muscles, 1–10 pg of rAAV genomes were detected by PCR, whereas 500 fg to 5 pg of rAAV sequences were amplified in the injected muscles of rAAV2-CMVLacZ (Figures 2b and 4b). These results indicate that the promoter-deleted rAAV2 could successfully infect canine muscles and the viral genomes were retained stably in the fibers.

H&E staining showed that deletion of the MCK promoter greatly reduced the cellular infiltration into the rAAV2-LacZ-P(−)-injected muscles at 2 and 4 weeks after the injection, in contrast to the rAAV2-CMVLacZ-injected muscles (Figure 4). Even in a muscle sample in which vector genome was detected at the highest level by PCR, infiltrating cells were rarely found (sample 1c in Figures 4b and c). In addition, CD4+ or CD8+ cells were not detected in the rAAV2-LacZ-P(−)-injected muscles (data not shown). These results suggest that the transgene product but not AAV particle strongly elicits immune responses that subsequently eliminated transduced myofibers.